Ion channel TRPV1-dependent activation of PTP1B suppresses EGFR-associated intestinal tumorigenesis

Petrus R. de Jong,[1,2] Naoki Takahashi,[1,3] Alexandra R. Harris,[1] Jihyung Lee,[1] Samuel Bertin,[1] James Jeffries,[1] Michael Jung,[1] Jen Duong,[1] Amy I. Triano,[1] Jongdae Lee,[1] Yaron Niv,[4] David S. Herdman,[1] Koji Taniguchi,[1,5] Chang-Whan Kim,[1,6] Hui Dong,[1] Lars Eckmann,[1] Stephanie M. Stanford,[7] Nunzio Bottini,[7] Maripat Corr,[1] and Eyal Raz[1]

[1]Department of Medicine, UCSD, La Jolla, California, USA. [2]University Medical Center Utrecht, Utrecht, The Netherlands. [3]Division of Oral Science for Health Promotion, Niigata University Graduate School of Medical and Dental Sciences, Niigata, Japan. [4]Department of Gastroenterology, Rabin Medical Center, affiliated with Sackler Faculty of Medicine, Tel Aviv University, Ramat Aviv, Israel. [5]Department of Microbiology and Immunology, Keio University School of Medicine, Tokyo, Japan. [6]The Catholic University of Korea, Seoul, Republic of Korea. [7]Division of Cellular Biology, La Jolla Institute for Allergy and Immunology, La Jolla, California, USA.

The intestinal epithelium has a high rate of turnover, and dysregulation of pathways that regulate regeneration can lead to tumor development; however, the negative regulators of oncogenic events in the intestinal epithelium are not fully understood. Here we identified a feedback loop between the epidermal growth factor receptor (EGFR), a known mediator of proliferation, and the transient receptor potential cation channel, subfamily V, member 1 (TRPV1), in intestinal epithelial cells (IECs). We found that TRPV1 was expressed by IECs and was intrinsically activated upon EGFR stimulation. Subsequently, TRPV1 activation inhibited EGFR-induced epithelial cell proliferation via activation of Ca^{2+}/calpain and resulting activation of protein tyrosine phosphatase 1B (PTP1B). In a murine model of multiple intestinal neoplasia ($Apc^{Min/+}$ mice), TRPV1 deficiency increased adenoma formation, and treatment of these animals with an EGFR kinase inhibitor reversed protumorigenic phenotypes, supporting a functional association between TRPV1 and EGFR signaling in IECs. Administration of a TRPV1 agonist suppressed intestinal tumorigenesis in $Apc^{Min/+}$ mice, similar to — as well as in conjunction with — a cyclooxygenase-2 (COX-2) inhibitor, which suggests that targeting both TRPV1 and COX-2 has potential as a therapeutic approach for tumor prevention. Our findings implicate TRPV1 as a regulator of growth factor signaling in the intestinal epithelium through activation of PTP1B and subsequent suppression of intestinal tumorigenesis.

Introduction

The mammalian intestinal epithelium reveals a complex interplay among intestinal stem cell (ISC) self-renewal in the crypts of Lieberkühn, progenitor cell proliferation, differentiation, and, ultimately, apoptosis (1). The high rate of intestinal epithelial cell (IEC) turnover within a genotoxic microenvironment needs to be tightly regulated to minimize the risk of neoplasia development from ISCs or dedifferentiated progenitor cells (2). The main drivers of IEC proliferation are the Wnt, Notch, and epidermal growth factor receptor (EGFR) pathways (3). Somatic mutations that result in gain of function of these and associated pathways are commonly found in colorectal cancer (CRC), underlining their oncogenic potential (4, 5). Similarly, whereas Toll-like receptor signaling in IECs provides essential proproliferative signals (6), these microbiota-induced signals also promote epithelial tumorigenesis (7). Microenvironmental cues that signal IECs to shift gears from a progenitor to a differentiated mode at the crypt-villus junction are instrumental in the regulation of crypt homeostasis (8). This includes the release of BMP and Hedgehog proteins along a spatial gradient. Interruption of this mesenchymal-epithelial crosstalk results in distortion of the crypt-villus architecture (9–11) and predisposes the epithelium to neoplasia (12, 13).

The regulatory role of physiological signals transduced by sensory ion channels in crypt homeostasis, and their implications for epithelial tumorigenesis, have not been fully studied. One exception is the reported homeostatic role of the stretch-activated receptor Piezo1. Overcrowding within the epithelial sheet is detected by the Piezo1 cation channel, which leads to live cell extrusion through Rho kinase activation, thereby keeping cell numbers in check. Interestingly, colonic polyps show increased cell densities in crypt sides compared with healthy epithelium, which suggests that aberrant cell extrusion may be an early oncogenic event in the intestines (14).

In the search for sensory receptors in epithelial tissues, the comprehensive family of TRP ion channels holds particular interest, as these sense and integrate a broad range of thermal, mechanical, and chemical environmental stimuli (15). The mammalian TRP family consists of multiple subfamilies, including canonical (TRPC), vanilloid (TRPV), melastatin (TRPM), ankyrin (TRPA), polycystin (TRPP), and mucolipin (TRPML), which form multimeric proteins that function as cation channels, display diverse gating mechanisms, and are ubiquitously expressed in various excitable and nonexcitable cell types (16). TRP channels are well represented in the complex milieu of the digestive tract (17). Moreover, various TRP channels are expressed in epithelial tissues (18, 19), and some data suggest that they promote cell proliferation

Conflict of interest: Hui Dong is cofounder of AddexBio.
Submitted: July 25, 2013; **Accepted:** June 6, 2014.
Reference information: *J Clin Invest*. 2014;124(9):3793–3806. doi:10.1172/JCI72340.

and may play a role in cellular transformation (20). Mechanistically, this has been shown to involve potentiation of EGFR signaling in other epithelial tissues, such as TRPV3 in keratinocytes (21) and TRPC1 in lung carcinoma cell lines (22). However, the physiological relevance of TRP-EGFR interactions and their associated signaling pathways in the intestinal epithelium are not known.

Here we demonstrate an unconventional role for the TRPV1 channel in intestinal crypt homeostasis and tumorigenesis. We found that TRPV1 was intrinsically activated by EGFR. Our molecular dissection showed that TRPV1 triggering subsequently initiated a molecular cascade — involving Ca^{2+}, calpain, and finally protein tyrosine phosphatase 1B (PTP1B) — that served as a negative feedback loop on EGFR activity. Deficiency of *Trpv1* resulted in IEC hyperproliferation in vivo and in intestinal organoid cultures in vitro, as well as increased formation of intestinal neoplasia. Collectively, our data suggest that TRPV1 is a nonredundant, intrinsic negative regulator of cell proliferation and intestinal tumorigenesis. Thus, rather than transducing physical signals, TRPV1 senses and regulates growth factor signaling in IECs in order to suppress intestinal tumorigenesis.

Results

TRPV1 is a functional Ca^{2+} channel in IECs and organoids. To evaluate the expression of TRPV family members in IECs, quantitative real-time RT-PCR (Q-PCR) screening for the abundance of *Trpv1–Trpv6* transcripts in both primary IEC isolates and intestinal organoids was performed. The latter is an autonomous IEC culture system that consists of self-organizing "miniguts" that recapitulate intestinal crypts, free of any potentially contaminating mesenchymal, neuronal, or bone marrow–derived cells (23). We found that *Trpv1*, *Trpv4*, *Trpv5*, and *Trpv6* were expressed in the intestinal epithelium, with similar expression patterns in freshly isolated IECs and intestinal organoid cultures (Figure 1, A and B, and Supplemental Figure 1, A and B; supplemental material available online with this article; doi:10.1172/JCI72340DS1). While the molecular effects of TRPV4 and TRPV5/TRPV6 in IECs have been reported previously (24, 25), the physiological role of TRPV1 in IEC biology is unknown. We validated expression of *Trpv1* mRNA in IECs using *Trpv1*$^{-/-}$ mice (26) for both organoid cultures and freshly isolated crypts (Supplemental Figure 1C). We also confirmed *TRPV1* mRNA expression in human and rodent IEC lines (Supplemental Figure 1D). To show TRPV1 protein expression, we first validated the specificity of the anti-TRPV1 Ab by using CHO cells that stably overexpress TRPV1 (Supplemental Figure 1, E and F). We confirmed TRPV1 expression in IECs using flow cytometry (Figure 1C). TRPV1 expression by primary IECs was demonstrated by immunofluorescent staining of intestinal organoids (Figure 1D). Staining with secondary antibody only (Alexa Fluor 488–conjugated anti-Rb) did not produce a positive signal (data not shown). We next evaluated TRPV1 ion channel functionality in IECs. As TRPV1 is primarily a Ca^{2+} channel (27), we first validated our experimental setup to measure cytosolic free Ca^{2+} ($[Ca^{2+}]_{cyt}$) measurements in cells loaded with Fura-2 acetoxymethyl ester (Fura-2 AM) (28, 29). We used CHO^{TRPV1} cells after stimulation with the TRPV1-specific agonist capsaicin (Supplemental Figure 1G). More importantly, addition of capsaicin induced $[Ca^{2+}]_{cyt}$ elevations in the IEC line HCT116 that were dose-dependent and abrogated by TRPV1 knockdown (Figure 1E). Pretreatment with the TRPV1 antagonist BCTC also inhibited capsaicin-induced Ca^{2+} influxes in HCT116 cells (Supplemental Figure 1H). Similar results were generated by applying heat as a TRPV1 activator (Figure 1F). To confirm the functionality of TRPV1 channels in primary IECs, we used intestinal organoids from WT and *Trpv1*$^{-/-}$ mice in the same experimental setup. Organoid-derived crypts were then stimulated with the TRPV1 agonist capsaicin, which resulted in marked $[Ca^{2+}]_{cyt}$ increases in WT, but not *Trpv1*$^{-/-}$, crypts (Figure 1, G–I). Collectively, these data demonstrated that TRPV1 is a functional Ca^{2+} channel in IECs.

Epithelial TRPV1 signaling inhibits EGFR activity in vivo. Next we used *Trpv1*$^{-/-}$ mice to evaluate the physiological function of TRPV1 signaling in IECs. TRPV1 deficiency did not significantly affect gross intestinal crypt-villus morphology or IEC differentiation (Supplemental Figure 2A). Consistent with these in vivo findings, we observed similar numbers of goblet and Paneth cells per crypt in intestinal organoids generated from WT and *Trpv1*$^{-/-}$ mice (Supplemental Figure 2B). In contrast, we observed a substantial increase in IEC proliferation in *Trpv1*$^{-/-}$ mice by immunostaining for Ki67, a marker of transient amplifying (TA) cells (Figure 2A). These data suggest that TRPV1 signaling negatively regulates epithelial cell proliferation. Since EGFR is a physiological inducer of IEC proliferation and has previously been associated with other TRP channels (21, 22), we hypothesized that the TRPV1 and EGFR signaling pathways may functionally interact. Constitutive phosphorylation of $EGFR^{Y1068}$, indicative of EGFR kinase activity, was increased in colonic crypts in *Trpv1*$^{-/-}$ mice (Figure 2, B–D). Moreover, *Trpv1*$^{-/-}$ crypts displayed increased constitutive phosphorylation of ERK1/2, a MAPK that relays downstream signaling of EGFR. This effect was reversed by treatment with the EGFR kinase inhibitor gefitinib (Figure 2B). Gefitinib also reversed the increased IEC proliferation in *Trpv1*$^{-/-}$ mice (Figure 2, E and F), which suggests that enhanced constitutive EGFR activation was responsible for the epithelial hyperproliferation observed in these mice. We then tested the effects of TRPV1 triggering on EGFR signaling in IECs in vivo. Expression levels of immediate early response genes reflect the transcriptional activity of EGFR signaling (30). A single oral administration of capsaicin (3 mg/kg) decreased expression levels of *c-Fos*, *Fosl2* (also known as *Fra2*), and *c-Jun* in WT mice, but not *Trpv1*$^{-/-}$ mice (Figure 2, G and H). Importantly, cotreatment with gefitinib (50 mg/kg) did not enhance the suppressive effect of capsaicin, which suggests that both agents optimally targeted the same pathway (i.e., EGFR). Oral administration of capsaicin also inhibited ligand-induced EGFR activation in IECs and suppressed epithelial cell proliferation (Supplemental Figure 2, C–E). Notably, oral capsaicin treatment did not significantly affect goblet or Paneth cell numbers (Supplemental Figure 2, F–H). Together, these results are suggestive of negative regulation of IEC proliferation and epithelial EGFR signaling by TRPV1.

In order to unambiguously address whether epithelial TRPV1 directly modulates EGFR kinase activity, we generated mice that overexpress TRPV1 (31) in IECs on the C57BL/6J background (referred to herein as $TRPV1^{IEC}$ mice). Excision of a stop sequence by Cre under the control of the Villin promoter resulted in conditional TRPV1 overexpression in IECs (Figure 2I). $TRPV1^{IEC}$ mice showed increased TRPV1 protein and mRNA expression in IECs,

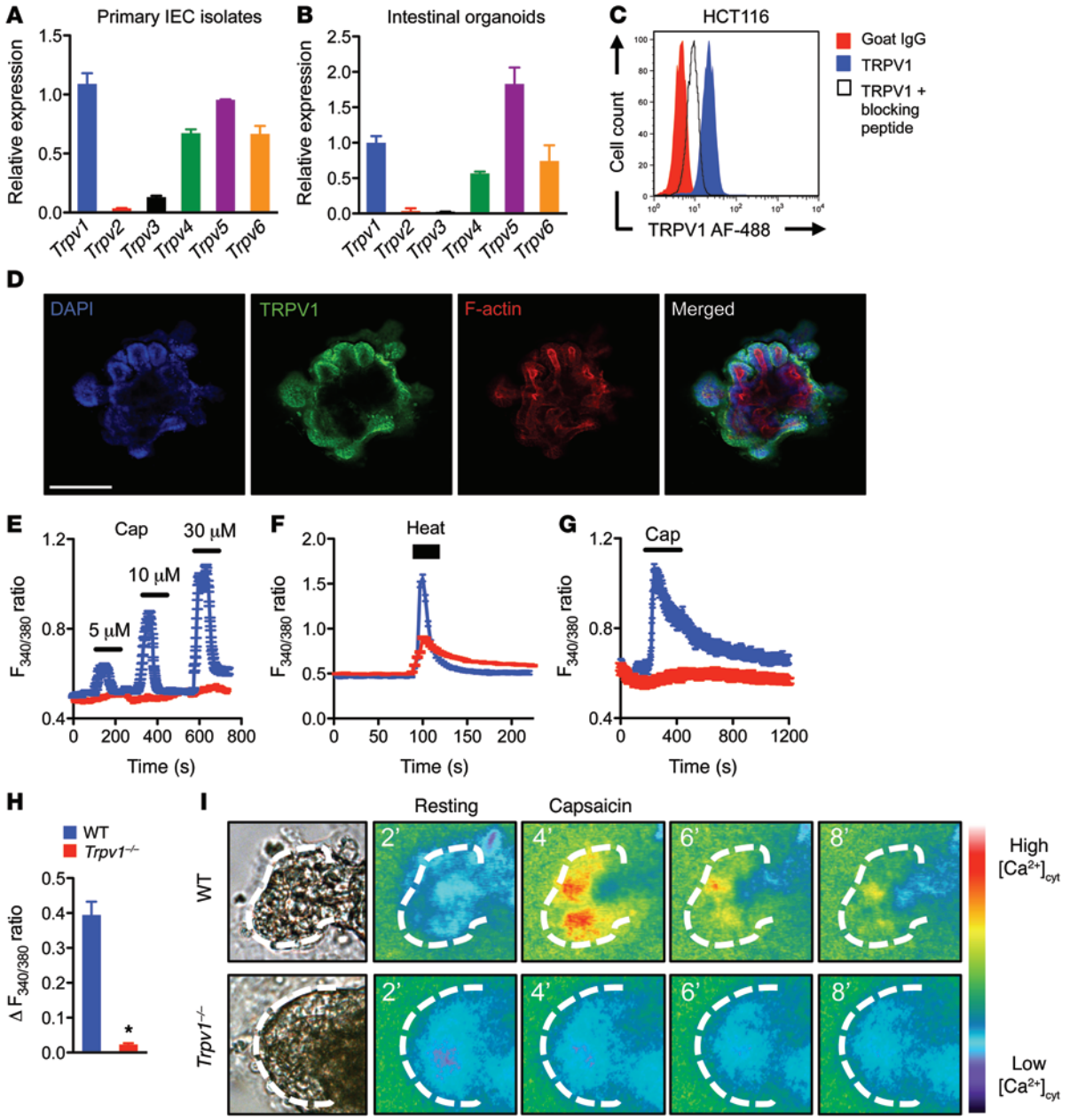

Figure 1. TRPV1 is a functional Ca^{2+} channel in IECs. (**A** and **B**) Transcript levels of *Trpv1*–*Trpv6* in (**A**) isolated crypts and (**B**) intestinal organoids, determined by Q-PCR and expressed relative to *Gapdh* control. Mean ± SD (n = 2). (**C**) Expression of TRPV1 by HCT116 cells, as determined by flow cytometry. Normal goat IgG and preabsorbed anti-TRPV1 Abs served as negative controls. (**D**) TRPV1 expression in intestinal organoids, shown by IF staining. Scale bar: 100 μm. (**E**) HCT116 shRNA control (blue line) or *TRPV1* shRNA knockdown (red line) cells were loaded with 5 μM Fura-2 AM and perfused with physiological salt solution (2 mM $CaCl_2$), followed by stimulation with 5–30 μm capsaicin (Cap) as indicated (black bars). Mean ± SEM (n = 50 cells per condition). (**F**) Fura-2 AM–loaded HCT116 control (blue) or *TRPV1* knockdown (red) cells were perfused with PSS at room temperature (20°C), then heated to 40°C (black bar). Mean ± SEM (n = 52 cells per condition). (**G**) Fura-2 AM–stained intestinal organoids generated from WT (blue line) or *Trpv1*$^{-/-}$ (red line) mice were stimulated with 30 μM capsaicin (black bar). Mean ± SEM (n = 25 regions per organoid). Representative results of 3 independent experiments. (**H**) Statistical analysis of the capsaicin-induced Ca^{2+} influx in **G**. Shown are averaged peak intracellular $[Ca^{2+}]$ levels after subtraction of baseline. Mean ± SEM (n = 25 per condition). *P < 0.001, t test. (**I**) Detailed images of organoid crypts (representative examples; original magnification, ×400) used for Ca^{2+} imaging, with colorimetric representation of low-to-high $[Ca^{2+}]_{cyt}$ measurements at the indicated time points.

but not in spinal cord homogenates (Supplemental Figure 3, A and B). Consistent with our results from *Trpv1*$^{-/-}$ mice, TRPV1^{IEC} animals showed reduced constitutive p-EGFR^{Y1068} levels in colon crypts, whereas total EGFR levels were unaffected (Figure 2J). Furthermore, IEC-specific TRPV1 overexpression suppressed EGF-induced EGFR activity in freshly isolated IECs, inhibited epithelial cell proliferation in vivo, and suppressed cell proliferation and expression of EGFR target genes in intestinal organoid cultures in vitro as well as the intensity of p-EGFR^{Y1068} staining (Figure 2K and Supplemental Figure 3, C–G). Collectively, these findings suggest that epithelial TRPV1 inhibits IEC proliferation by antagonizing EGFR signaling.

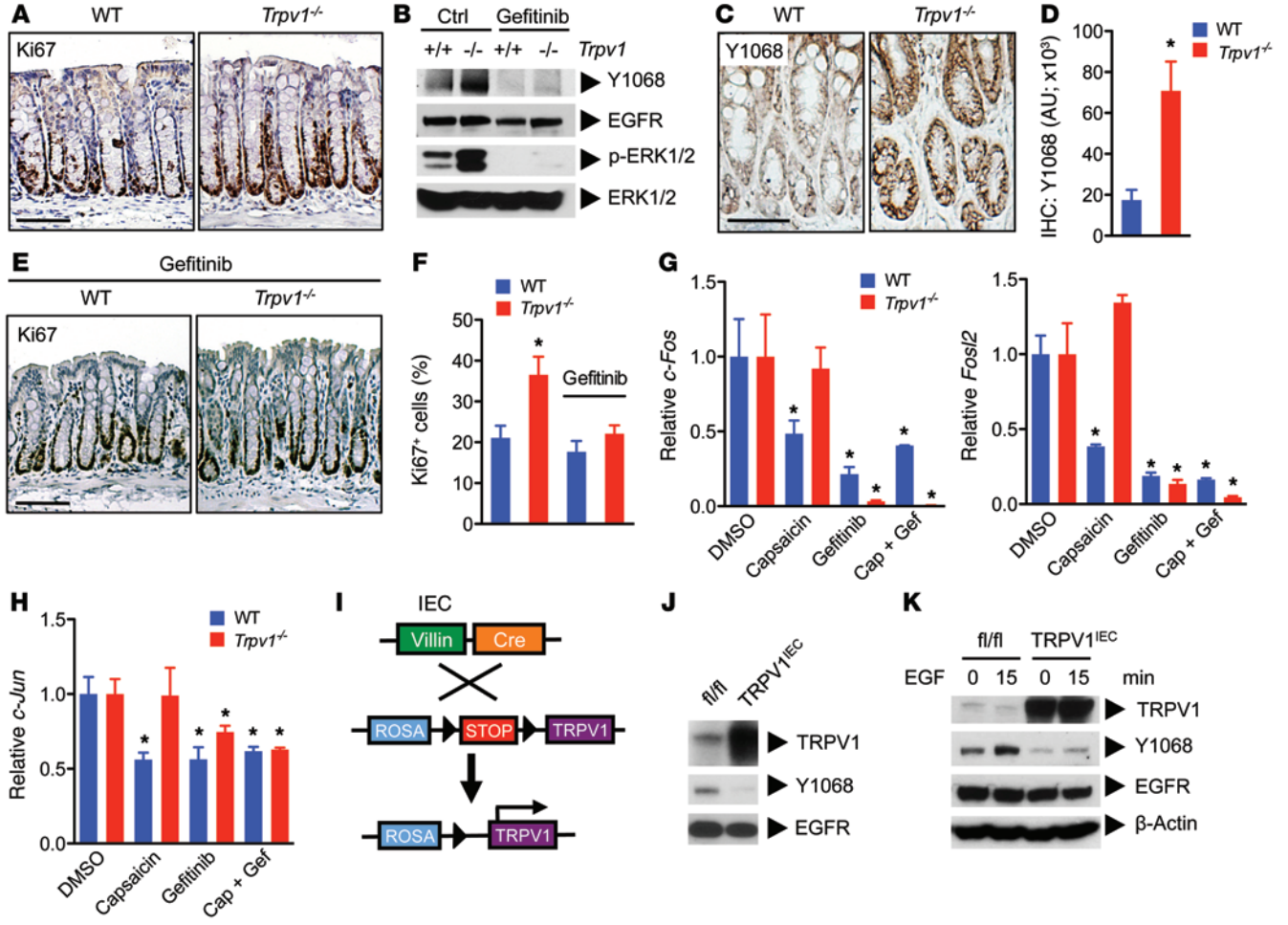

Figure 2. TRPV1 signaling inhibits cell proliferation and EGFR activity in vivo. (**A**) Increased IEC proliferation in colons from naive *Trpv1*$^{-/-}$ versus WT mice, as shown by Ki67 immunostaining. (**B**) Increased EGFR^{Y1068} phosphorylation in *Trpv1*$^{-/-}$ IECs was reversed by gefitinib treatment. Mice were treated with 2 doses of gefitinib (50 mg/kg, gavage) with a 6-hour interval, followed by IEC harvesting and Western blotting. Shown are representative results from 3 experiments. (**C**) Immunostaining for p-EGFR^{Y1068} of distal colon tissues. (**D**) Quantification with ImageJ. 3 representative areas were used for analysis, with 3 mice per group. (**E**) Hyperproliferation of *Trpv1*$^{-/-}$ IECs was reversed by EGFR inhibition with gefitinib (50 mg/kg) for 5 consecutive days before tissue harvesting. (**F**) Quantification of Ki67^{+} cells by ImageJ (ImmunoRatio plugin). (**G**) Capsaicin administration suppressed transcription of EGFR target genes in a TRPV1-dependent manner, comparable to gefitinib. Mice received DMSO, capsaicin (3 mg/kg), gefitinib (50 mg/kg), or capsaicin plus gefitinib by gavage, and IECs were prepared 6 hours later. Shown is Q-PCR analysis for *c-Fos* or *Fosl2*, relative to the respective DMSO control. (**H**) Q-PCR analysis for *c-Jun*. (**I**) Generation of transgenic TRPV1^{IEC} mice. (**J**) TRPV1$^{fl/fl}$ and TRPV1^{IEC} mice were analyzed for p-EGFR^{Y1068} by Western blotting. IEC-specific TRPV1 overexpression inhibited constitutive EGFR signaling in IECs. (**K**) IEC-specific TRPV1 overexpression suppressed EGF-induced EGFR^{Y1068} phosphorylation in IECs. Data are mean ± SEM (**D** and **F**; n = 3 per group) or mean ± SD (**G** and **H**; n = 2 per group). *$P < 0.05$, t test (**D**) or ANOVA (**F**–**H**). Scale bars: 100 μm.

TRPV1 intrinsically inhibits EGFR signaling and epithelial cell proliferation. We then further explored the molecular interactions between TRPV1 and EGFR in vitro. Similar to the data derived from TRPV1^{IEC} transgenic mice, overexpression of TRPV1 in HCT116 cells inhibited ligand-induced EGFR^{Y1068} phosphorylation compared with mock-transfected cells (Figure 3A). This was recapitulated in CHO cells with reconstituted expression of WT-EGFR, with or without TRPV1 (Supplemental Figure 4A). Exploration of other EGFR phosphorylation sites showed that TRPV1 suppressed phosphorylation of Y992 and Y1045, in addition to Y1068, but not S1046/S1047 (Supplemental Figure 4B). Since the Y1068 phosphorylation site was a more robust readout, and is associated with multiple proproliferative signaling pathways, we focused on phospho-EGFR^{Y1068} levels in subsequent assays. Stable knockdown of TRPV1 in HCT116 cells by shRNA (validated in Figure 1, E and F) resulted in enhanced ligand-induced EGFR^{Y1068} phosphorylation (Figure 3B). This effect coincided with an increased rate of cell proliferation, which was reversed by gefitinib treatment (Figure 3C). These data further support the functional and intrinsic association between the TRPV1 and EGFR signaling pathways in IECs.

To compare the effects of the TRPV1 channel with those of other TRPV family members that we found to be expressed by IECs, we repeated our in vitro assays for the thermosensors TRPV3 and TRPV4, as well as the Ca^{2+} transporter TRPV5. Overexpression of TRPV3 potentiated ligand-induced EGFR^{Y1068} phosphorylation in HCT116 cells (consistent with previous findings in keratinocytes; ref. 21), whereas TRPV4 overexpression had no significant effects (Supplemental Figure 4C). Interestingly, like TRPV1, TRPV5 significantly suppressed ligand-induced EGFR^{Y1068} phosphorylation (Supplemental Figure 4, D and E). These data suggest a more gen-

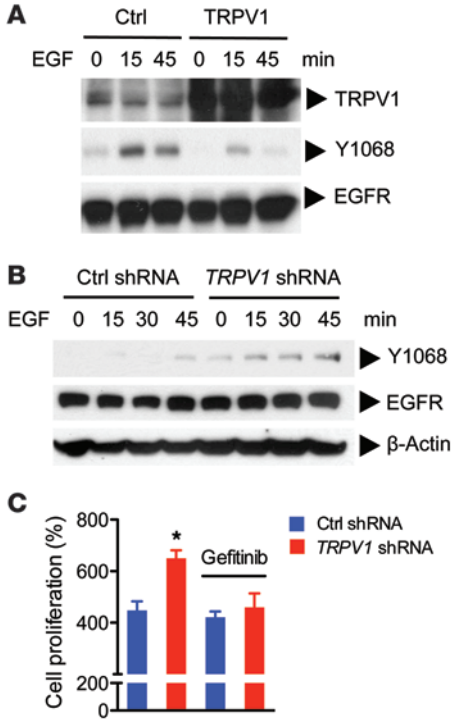

Figure 3. TRPV1 inhibits epithelial cell proliferation and EGFR signaling in vitro. (**A**) Overexpression of TRPV1 inhibited EGF-induced EGFR activity in the IEC line HCT116. Cells were transfected with control or TRPV1 plasmid and stimulated with 1 ng/ml EGF for the indicated times, followed by Western blot analysis of total cell lysates. (**B**) TRPV1 knockdown enhanced EGFR signaling in IECs in vitro. HCT116 cells were transfected with control or *TRPV1* shRNA. After obtaining stable cell lines, control and knockdown cells were stimulated with low-dose EGF (1 ng/ml) for the indicated times, and cell lysates were analyzed by Western blotting. (**C**) HCT116 cells treated with control or *TRPV1* shRNA were cultured for 3 days in the presence or absence of gefitinib (1 μM). Cells were then analyzed for cell proliferation with the MTT assay. Results are presented as a percentage of day 1 of cell culture. Mean ± SEM. **P* < 0.05 vs. control, ANOVA.

eral role for TRP channel–mediated Ca^{2+} influx in the regulation of EGFR signaling in IECs. However, as these effects might occur by different mechanisms, we focused in subsequent experiments on dissecting the TRPV1-mediated effects on EGFR signaling.

Physiological effects of epithelial TRPV1 signaling in intestinal organoids. To substantiate our findings on TRPV1 in a more physiological setting, we studied the growth kinetics of intestinal organoids derived from WT and *Trpv1*$^{-/-}$ mice. Mature *Trpv1*$^{-/-}$ organoids produced larger crypts compared with WT controls under similar culture conditions (Figure 4, A and B). Q-PCR analysis of *Mki67* transcripts showed significantly increased expression in *Trpv1*$^{-/-}$ organoids, which was confirmed by immunostaining (Figure 4, C–E, and Supplemental Figure 5, A–C). Moreover, this increased proliferation coincided with increased expression of the EGFR target gene *c-Fos* in *Trpv1*$^{-/-}$ organoids (Figure 4F). We then hypothesized that *Trpv1*$^{-/-}$ organoids would have a reduced requirement for exogenous EGF, as recently reported for another negative regulator of EGFR signaling, leucine-rich and immunoglobulin-like domains protein 1 (Lrig1; ref. 32). Indeed, WT organoids showed an almost complete loss of proliferation in the absence of exogenous EGF, whereas *Trpv1*$^{-/-}$ organoids maintained active TA cells under the same conditions (Figure 4, G and H, and Supplemental Figure 5D). Consistent with our in vivo findings, these data suggest that TRPV1 is an intrinsic regulator of EGFR signaling in IECs, acting to confine the proliferating cell compartment in the intestinal crypt.

TRPV1 regulates EGFR through Ca^{2+}/calpain and PTP1B. To identify the molecular mechanism by which TRPV1, a nonselective Ca^{2+} channel, regulates EGFR activity, we explored the involvement of Ca^{2+}-dependent effectors, including the calmodulin, calcineurin, and calpain pathways (20). Calmodulin-dependent kinase II–mediated (CaMKII-mediated) Ser phosphorylation of the intracellular tail of EGFR can inhibit EGFR kinase activity (33), which we indeed found to be enhanced in TRPV1-overexpressing cells (Supplemental Figure 4B). However, even though the CaM inhibitor W-7 efficaciously blocked ionomycin-induced CaMKII activation, pretreatment with W-7 did not reverse the inhibitory effects of TRPV1 overexpression on $EGFR^{Y1068}$ phosphorylation (Supplemental Figure 6, A and B). Similarly, and despite the reported inhibitory role of Ca^{2+}/calcineurin activity on EGFR signaling (34), calcineurin inhibition by FK506 failed to reverse the TRPV1-mediated effects on $EGFR^{Y1068}$ phosphorylation (Supplemental Figure 6, C and D).

We then focused on the Ca^{2+}/calpain pathway. Regulation of $EGFR^{Y1068}$ phosphorylation by TRPV1 was prevented by pretreatment with the cell-permeable calpain inhibitor ALLM (Figure 5A), suggestive of direct or indirect inhibitory effects of calpain on EGFR kinase activity. Dephosphorylation of EGFR by protein tyrosine phosphatases (PTPs) is an important early regulatory loop that controls receptor tyrosine kinase signaling (35). Since there is no evidence in the literature for direct posttranslational modulation of the EGFR by calpain, we hypothesized that calpain might control the activity of a PTP, which in turn regulates the phosphorylation status of EGFR. Indeed, pretreatment with the nonspecific PTP inhibitor sodium orthovanadate (Na_3VO_4) reversed the negative regulatory effect of TRPV1 on $EGFR^{Y1068}$ phosphorylation (Figure 5B). PTPs that are known to regulate EGFR kinase activity include LAR (encoded by *Ptprf*), PTP-σ (*Ptprs*), PTP1B (*Ptpn1*), TCPTP (*Ptpn2*), and SHP-1 (*Ptpn6*) (36). We found all of these PTPs to be expressed by IECs (Figure 5C), although their expression levels were similar in WT and *Trpv1*$^{-/-}$ mice (Supplemental Figure 6E). Of these PTP candidates, only PTP1B is known to be functionally associated with Ca^{2+}/calpain (37). Posttranslational cleavage of PTP1B by calpain increases its phosphatase activity (38). Accordingly, pretreatment with the cell-permeable PTP1B inhibitor Compound 3 recapitulated the effect of Na_3VO_4 in reversing TRPV1-mediated dephosphorylation of EGFR (Figure 5B). The crucial role of this PTP in the TRPV1-mediated effects on EGFR was confirmed by siRNA-mediated knockdown of *PTP1B* (Figure 5D). Another target of PTP1B upon EGF stimulation is the early endosomal protein hepatocyte growth factor–regulated tyrosine kinase substrate (Hrs) (39). TRPV1-mediated Ca^{2+} influx and subsequent calpain activation should therefore also affect Hrs^{Y334} phosphorylation, the major phosphorylated tyrosine residue in response to EGF (40). Indeed, we found that overexpression of TRPV1 resulted in suppression of Hrs^{Y334} phosphorylation upon EGF stimulation (Supplemental Figure 6F). Finally, to confirm

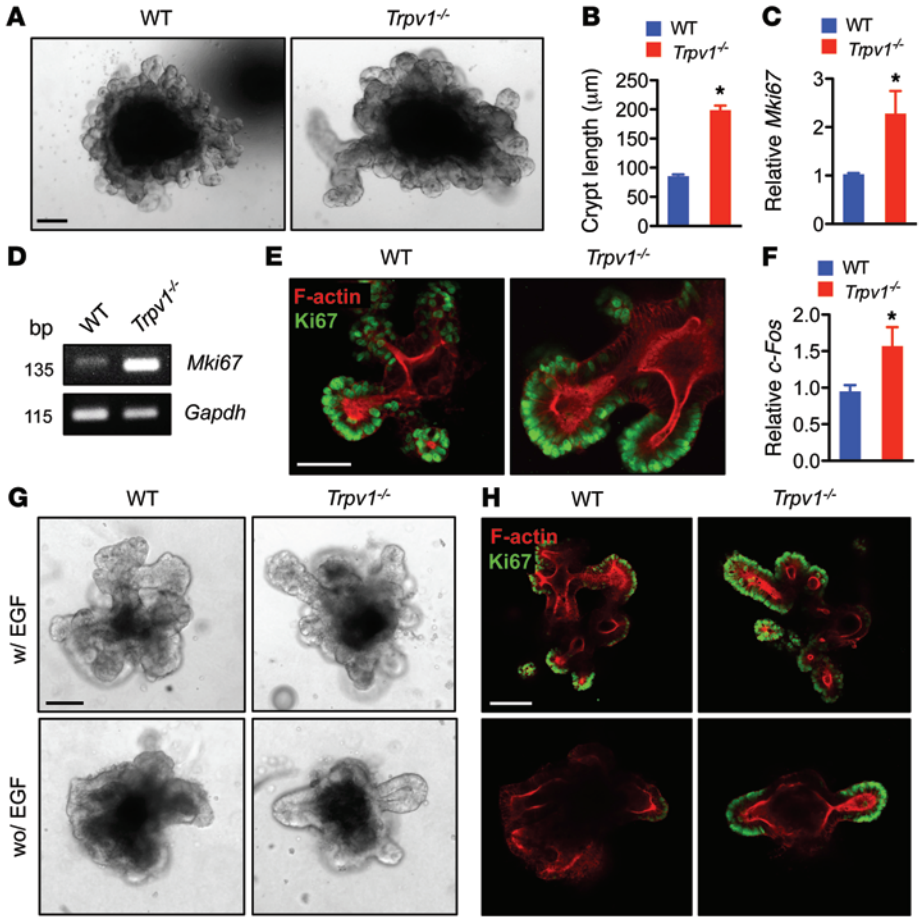

Figure 4. Physiological effects of TRPV1 signaling in intestinal organoids. (**A**) Representative live-cell microscopy images of small intestinal organoids generated from WT and *Trpv1*$^{-/-}$ mice at day 7 after passing. (**B**) Quantification of crypt lengths of WT and *Trpv1*$^{-/-}$ organoids (n = 8). (**C**) Expression of the proliferation marker *Mki67* in WT and *Trpv1*$^{-/-}$ organoids, determined by Q-PCR and expressed relative to WT (n = 3). (**D**) Increased *Mki67* expression in *Trpv1*$^{-/-}$ versus WT organoids. (**E**) Immunostaining for Ki67 of WT and *Trpv1*$^{-/-}$ organoids showed an increase in the proliferative zone in the latter. Confocal fluorescence microscopy is shown. (**F**) Q-PCR analysis of *c-Fos* expression in WT and *Trpv1*$^{-/-}$ organoids, normalized to *Gapdh* and expressed relative to WT (n = 3 per group). (**G**) TRPV1 deficiency reduced the exogenous EGF requirement of intestinal organoids. WT and *Trpv1*$^{-/-}$ organoids were cultured with standard medium with or without EGF (50 ng/ml) for 48 hours. Representative images of organoids by brightfield microscopy are shown. (**H**) Organoids as in **G**, stained for Ki67 and F-actin. Scale bars: 50 μm (**E**); 100 μm (**A**, **G**, and **H**). Mean ± SEM. *$P < 0.05$, Student's t test. Data representative of 2–3 independent experiments.

that calpain-mediated cleavage of PTP1B between amino acid residues 360–380 enhances its intrinsic phosphatase activity (38), we transfected HCT116 cells with PTP1B WT (PTP435) or C-terminal truncated mutants (PTP370 and PTP377). Expression of PTP1B truncation mutants (Supplemental Figure 6G) resulted in reduced EGF-induced phospho-EGFR^{Y1068} levels (Figure 5E). Together, these data support a functional role between TRPV1 and PTP1B and suggest that both are essential components of a negative regulatory loop of EGFR in IECs.

Functional PTP1B activity was previously reported to mediate differential responses to ligand-induced activation versus transactivation of the EGFR in IEC lines (41). However, the expression pattern of PTP1B in primary IECs is unknown. We found expression of PTP1B in budding crypts in small intestinal organoids and confirmed this in primary tissues by immunohistochemistry (Figure 5, F and G). We then characterized PTP1B expression along the crypt-villus axis by Q-PCR. IEC fractionation showed that TRPV1 and PTP1B were relatively enriched in the crypt compartment (Figure 5H). The IEC fractionation was validated by showing enrichment for the ISC marker *Lgr5*, the Paneth cell marker *Mmp7*, *Egfr*, and the EGFR target gene *Egr1* in the crypt fraction, with decreasing expression of the mature enterocyte marker *Slc26a3* (Supplemental Figure 6H). Collectively, these data are suggestive of an intrinsic, negative regulatory pathway through TRPV1 via Ca^{2+}/calpain and PTP1B on EGFR signaling in the intestinal crypt.

EGFR and TRPV1 are part of a homeostatic molecular circuit. The activity of certain TRP channels can be potentiated by phospholipase C–coupled (PLC-coupled) receptor tyrosine kinases (15). One of the proposed models of TRP activation is the release from its tonic inhibition by membrane lipids, such as phosphatidylinositol-4,5-bisphosphate (PIP_2). Hydrolysis of PIP_2 in the plasma membrane, for example by PLC-coupled receptors, would thereby reduce the threshold for TRPV1 activation (42, 43). As ligand-induced triggering of EGFR results in rapid PLCγ1-mediated PIP_2 hydrolysis in the plasma membrane (44), we hypothesized that EGFR activation might therefore facilitate TRPV1 gating. To test this hypothesis, we transfected cells with EGFR and/or TRPV1 and measured intracellular [Ca^{2+}] after EGF stimulation. We found that expression of EGFR or TRPV1 alone did not result in EGF-induced $[Ca^{2+}]_{cyt}$ increases in CHO or HEK293 cells (Figure 6, A and C). However, coexpression of EGFR and TRPV1 resulted in EGF-induced Ca^{2+} responses in both cell types (Figure 6, B and D). This functional coupling between EGFR and TRPV1 was abrogated by addition of exogenous PIP_2 or by *PLCG1* knockdown (Figure 6, B and D). Knockdown of PLCγ1 was validated by Western blotting (Supplemental Figure 7A). Together, these data support a model in which EGFR activation results in PLC-mediated TRPV1 triggering, followed by intracellular Ca^{2+} mobilization and activation of calpain and PTP1B. PTP1B subsequently dephosphorylates EGFR, thereby completing the negative feedback loop (Supplemental Figure 7B).

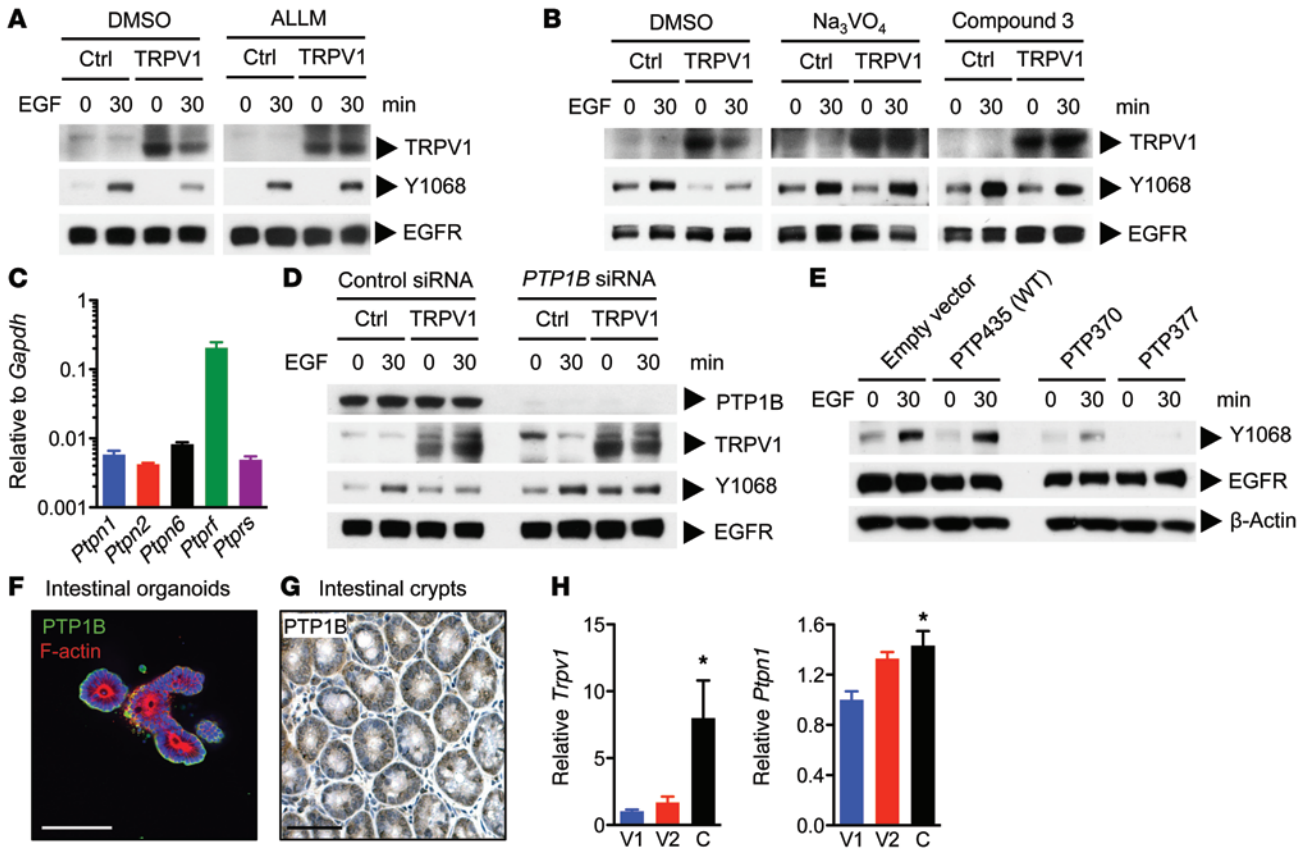

Figure 5. TRPV1 regulates EGFR activity through calpain and PTP1B. (**A**) HCT116 cells were transfected with control or TRPV1 plasmid, then pretreated with DMSO or ALLM (10 μM) for 1 hour, followed by EGF (1 ng/ml) stimulation. Total cell lysates were analyzed by Western blotting. Lanes were run on the same gel. (**B**) HCT116 cells transfected with control or TRPV1 plasmid were pretreated with DMSO, the nonselective PTP inhibitor Na_3VO_4 (10 μM), or the selective PTP1B inhibitor Compound 3 (10 μM) for 1 hour, followed by EGF stimulation and Western blotting. (**C**) Q-PCR was performed for PTP candidates with RNA isolated from WT colon crypts. (**D**) HCT116 cells were treated with control or *PTP1B* siRNA and transfected with control or TRPV1 plasmid. Cells were then stimulated with EGF (1 ng/ml) and analyzed by Western blotting. Representative results of 2 independent experiments. (**E**) HCT116 cells were transfected with empty vector, WT PTP1B (PTP435), or PTP1B C-terminal truncation mutants (PTP370 and PTP377). Cells were stimulated with EGF (1 ng/ml) and analyzed by Western blotting. Representative results of 3 independent experiments. (**F**) PTP1B expression in intestinal organoids, shown by confocal fluorescent microscopy. (**G**) Expression of PTP1B in murine small intestinal tissue sections. Immunostaining for PTP1B and detection with DAB (brown) was followed by counterstaining with hematoxylin. (**H**) Q-PCR analysis of villus (V1 and V2) and crypt (C) fractions for *Trpv1* and *Ptpn1*, showing enrichment in the latter. Values are expressed relative to the V1 fraction. Mean ± SEM (n = 3 per group). *$P < 0.05$, ANOVA. Scale bars: 100 μm.

TRPV1 signaling inhibits the development of intestinal neoplasia. EGFR signaling accelerates the development of neoplasia in mice genetically susceptible to intestinal adenoma formation (i.e., $Apc^{Min/+}$ mice; ref. 45). Given these tumor-promoting properties of EGFR signaling and the data presented above, we hypothesized that genetic deletion of *Trpv1* would promote the development of intestinal neoplasia. As predicted, $Apc^{Min/+}$ mice crossed with $Trpv1^{-/-}$ mice developed significantly more tumors in the intestinal tract, in accordance with recent data (46), an effect that was prevented by gefitinib treatment (Figure 7, A and B). This was associated with increased morbidity in $Apc^{Min/+}$ $Trpv1^{-/-}$ versus $Apc^{Min/+}$ mice, as shown by decreased levels of blood hemoglobin (HgB) as well as reduced lifespan (Figure 7, C and D). We observed increased constitutive $EGFR^{Y1068}$ phosphorylation and elevated expression of the proliferation marker PCNA in IECs from $Apc^{Min/+}$ $Trpv1^{-/-}$ mice, which was reversed by gefitinib treatment (Figure 7E). The epithelial hyperproliferation in $Apc^{Min/+}$ $Trpv1^{-/-}$ versus $Apc^{Min/+}$ mice was confirmed by Ki67 staining (Figure 7F). Furthermore, deletion of *Trpv1* resulted in significantly increased expression levels of the EGFR-regulated oncogenes *c-Fos* and *c-Myc* on the $Apc^{Min/+}$ background, without affecting the Wnt target *Axin2* (Figure 7G and Supplemental Figure 8, A and B). These findings support the concept that increased constitutive EGFR signaling in $Apc^{Min/+}$ $Trpv1^{-/-}$ mice predisposed this strain to develop more intestinal neoplasia.

Given the potential role of TRPV1-expressing sensory neurons in the regulation of intestinal tumorigenesis, we also evaluated the phenotype of $Apc^{Min/+}$ mice that underwent systemic ablation of $TRPV1^+$ neurons. $Apc^{Min/+}$ mice were treated with the ultrapotent TRPV1 agonist resiniferatoxin (RTX) during the neonatal period (47). Ocular challenge with capsaicin (eye wipe test) confirmed systemic $TRPV1^+$ sensory neuron ablation. In contrast to mice with global deletion of *Trpv1*, the RTX-treated mice showed a slight survival benefit, whereas intestinal tumor counts and HgB levels were comparable to those of $Apc^{Min/+}$ mice (Supplemental Figure 8, C and D). Thus, these results indirectly substantiate the tumor-suppressive role of epithelial TRPV1 in the intestines.

Finally, administration of the dietary TRPV1 agonist capsaicin, mixed at 0.01% (w/w) with chow, significantly increased the sur-

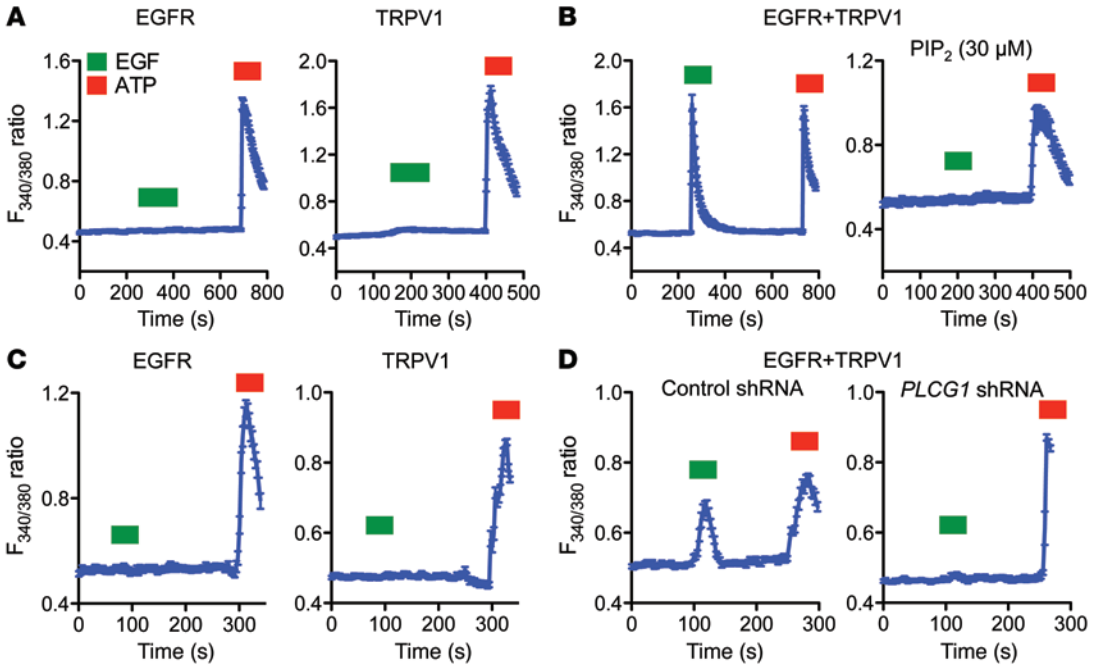

Figure 6. EGFR and TRPV1 are part of a homeostatic circuit. (**A**) EGFR triggering induced TRPV1-mediated Ca^{2+} influx. CHO cells did not show Ca^{2+} influxes in response to EGF (100 ng/ml; green bars) when only EGFR or TRPV1 was expressed (n = 43 and 42, respectively). ATP (10 μM; red bars) served as a positive control. (**B**) CHO cells expressing both EGFR and TRPV1 showed $[Ca^{2+}]_{cyt}$ increases in response to EGF stimulations, which was prevented by addition of exogenous PIP_2 (n = 50 and 52, respectively). (**C**) HEK293 cells did not show EGF-induced Ca^{2+} responses in the presence of only EGFR or TRPV1 (n = 50 per condition). (**D**) HEK293 cells showed $[Ca^{2+}]_{cyt}$ increases in response to EGF when EGFR and TRPV1 were coexpressed, which was prevented by *PLCG1* knockdown (n = 50 and 52, respectively). HEK293 cells were transfected with control or *PLCG1* siRNA, together with EGFR and TRPV1 expression plasmids. Ca^{2+} imaging was performed at day 3 after transfection. Mean ± SEM from individual $[Ca^{2+}]_{cyt}$ measurements of Fura-2 AM–loaded cells, representative of 2 (**B** and **D**) or 3 (**A** and **C**) independent experiments.

vival of $Apc^{Min/+}$ mice, an effect that was TRPV1 dependent (median survival, $Apc^{Min/+}$ fed regular diet, 23.2 weeks; $Apc^{Min/+}$ fed capsaicin diet, 31.5 weeks; $Apc^{Min/+}$ $Trpv1^{-/-}$ fed regular diet, 20 weeks; $Apc^{Min/+}$ $Trpv1^{-/-}$ fed capsaicin diet, 19.5 weeks; Figure 7D). This survival benefit was comparable to that achieved with the COX-2 inhibitor celecoxib (Figure 7H), an effective drug for the chemoprevention of CRC (48). In this setting, one of the proposed mechanisms of COX-2 inhibitors is suppression of EGFR transactivation via the COX product prostaglandin E_2 (49). Importantly, dietary treatment of $Apc^{Min/+}$ mice with both TRPV1 agonist and COX-2 inhibitor further prolonged survival, lowered intestinal tumor burden, and reduced tumor-related morbidity (Figure 7, H–J). Median survival of $Apc^{Min/+}$ mice treated with regular diet, celecoxib diet, and celecoxib plus capsaicin diet was 22, 29, and 45.2 weeks, respectively. Taken together, these data suggest that TRPV1 activation restrains EGFR signaling in the intestinal crypt and thereby minimizes the risk of neoplasia development.

Discussion

Here we propose that TRPV1 plays an indispensable role in the intestinal epithelium as an intrinsic regulator of growth factor receptor signaling, cell proliferation, and tumorigenesis. In this context, epithelial TRPV1 may be activated independently from its classical agonists: heat, capsaicin, lipid mediators, oxidative agents, and low pH (50–52). Our results suggest a different mode of activation of TRPV1, by PLCγ-mediated depletion of PIP_2, a tonic negative regulator of TRPV1, after receptor tyrosine kinase activation (42, 43). This proposed PLCγ-PIP_2-TRPV1 signaling axis was initially inferred from the observation that activation of TrkA sensitizes TRPV1 to physical or chemical stimuli (53). More recently, others showed that activation of another receptor tyrosine kinase, c-Met, evoked TRPV1 channel activity in hepatocytes (54). Our present findings are consistent with a model in which receptor tyrosine kinases functionally interact with TRPV1. Moreover, our data suggest that the physiological role of TRPV1 in the intestinal epithelium is to restrain EGFR signaling. This negative feedback downstream of TRPV1 is dependent on the intracellular actions of Ca^{2+}/calpain and a phosphatase (PTP1B), regulates the proliferation rate of IECs, and suppresses intestinal tumorigenesis. The proposed molecular pathway and its in vivo relevance are summarized in Figure 8.

Incidentally, we also found the TRPV5 Ca^{2+} channel to be capable of suppressing ligand-induced EGFR activation (Supplemental Figure 4E). TRPV5 is potentiated by PIP_2, in contrast to TRPV1 (55), suggestive of a distinct mechanistic link between TRPV5 and EGFR that remains to be elucidated (Supplemental Figure 9). The highly selective TRPV5 Ca^{2+} channel has been described to be involved in transcellular absorption of Ca^{2+} in the intestines, osteoclastic Ca^{2+} resorption of bone tissue, as well as active Ca^{2+} reabsorption in the kidneys (56). Thus, TRPV5 also exerts many extraintestinal effects in the regulation of Ca^{2+} homeostasis. A functional relationship with the EGFR pathway, such as that previously described for the Mg^{2+} channel TRPM6 in distal convoluted tubule cells of the kidney (56, 57), has not been reported for

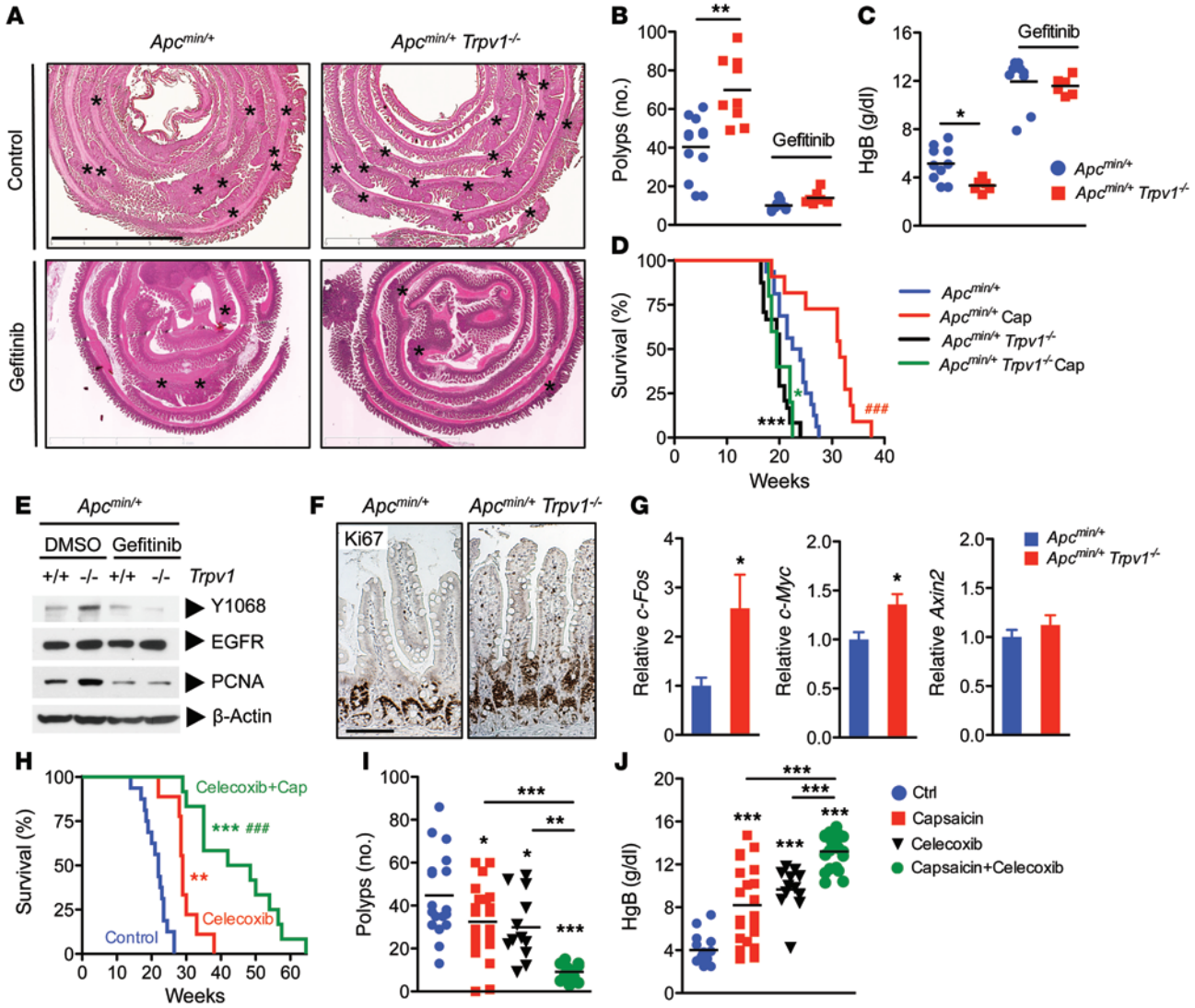

Figure 7. TRPV1 signaling inhibits intestinal neoplasia development. (**A**) Increased tumor burden in $Apc^{Min/+}$ $Trpv1^{-/-}$ mice. Shown are representative examples of small intestinal polyps (asterisks) in untreated and gefitinib-treated $Apc^{Min/+}$ and $Apc^{Min/+}$ $Trpv1^{-/-}$ mice. Scale bar: 4 mm. (**B**) 10-week-old $Apc^{Min/+}$ and $Apc^{Min/+}$ $Trpv1^{-/-}$ mice were treated with gefitinib (50 mg/kg/d) until 20 weeks, and polyps (>1 mm) were counted. n = 12 (untreated $Apc^{Min/+}$), 9 (gefitinib-treated $Apc^{Min/+}$ and untreated $Apc^{Min/+}$ $Trpv1^{-/-}$), 7 (gefitinib-treated $Apc^{Min/+}$ $Trpv1^{-/-}$). (**C**) HgB levels at 20 weeks. (**D**) Survival curves of $Apc^{Min/+}$ and $Apc^{Min/+}$ $Trpv1^{-/-}$ mice, treated with normal chow (n = 16 and 24, respectively) or capsaicin (Cap; n = 11 and 5, respectively). $^{###}P$ = 0.0004, $Apc^{Min/+}$ capsaicin vs. $Apc^{Min/+}$; $^{***}P$ = 0.0003, $Apc^{Min/+}$ $Trpv1^{-/-}$ vs. $Apc^{Min/+}$; P = NS, $Apc^{Min/+}$ $Trpv1^{-/-}$ vs. $Apc^{Min/+}$ $Trpv1^{-/-}$ capsaicin; $^{*}P$ = 0.019, $Apc^{Min/+}$ $Trpv1^{-/-}$ capsaicin vs. $Apc^{Min/+}$, log-rank test. (**E**) Increased p-EGFR^{Y1068} and PCNA levels in $Apc^{Min/+}$ $Trpv1^{-/-}$ colon crypts was reversed by gefitinib treatment, as in Figure 2B. (**F**) Increased IEC proliferation in $Apc^{Min/+}$ $Trpv1^{-/-}$ mice. Scale bar: 100 μm. (**G**) Expression of EGFR- and Wnt-regulated genes in IEC lysates from 15-week-old $Apc^{Min/+}$ and $Apc^{Min/+}$ $Trpv1^{-/-}$ mice (n = 9 and 5, respectively). Mean ± SEM, expressed relative to $Apc^{Min/+}$. $^{*}P < 0.05$, t test. (**H**) $Apc^{Min/+}$ mice were treated with regular chow (n = 16; different cohort from **D**), chow mixed with 300 ppm celecoxib (n = 9), or celecoxib plus capsaicin (n = 12). $^{**}P < 0.001$, celecoxib vs. control; $^{***}P < 0.0001$, celecoxib+capsaicin vs. control; $^{###}P$ = 0.0002, celecoxib+capsaicin vs. celecoxib, log-rank test. (**I**) Polyp counts and (**J**) HgB levels at 20 weeks. $^{*}P < 0.05$, $^{**}P < 0.001$, $^{***}P < 0.0001$ vs. control or as indicated, ANOVA (**B**, **C**, **I**, and **J**).

TRPV5. Needless to say, the association between TRPV5 and the EGFR needs to be further addressed. Furthermore, given the high expression levels of TRPV5 in IECs, the potential physiological role of TRPV5 with regard to EGFR signaling should be directly compared with that of TRPV1 to evaluate whether mechanistic differences exist between these TRP channels.

The dynamic events within the intestinal crypt include pro-proliferative signals from the crypt base (i.e., Wnt and Notch) that are counteracted by negative regulatory signals at the crypt-villus junction (8). EGFR signaling represents a third pathway that promotes cellular growth and the development of colorectal neoplasia (58). To prevent sporadic tumorigenesis, EGFR activation is coupled to the prompt initiation of cell-intrinsic inhibitory mechanisms, including dephosphorylation by PTP, receptor endocytosis, and the transcriptional upregulation of a variety of inhibitors (59). An example of the latter is the pan-ErbB inhibitor Lrig1, which promotes EGFR degradation (60). Importantly, Lrig1 was recently shown to be a physiological regulator of EGFR signaling in the intestinal crypt (32). Genetic deletion of *Lrig1* not only leads to crypt expansion, but also unleashes the oncogenic potential of

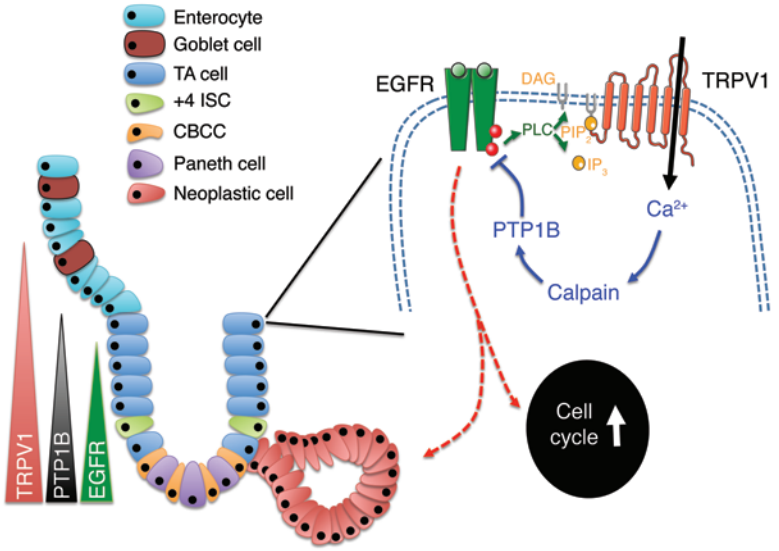

Figure 8. Proposed model for EGFR-TRPV1 crosstalk in IECs. TRPV1 and PTP1B are part of a homeostatic signaling circuit that restrains EGFR-induced epithelial cell proliferation. EGFR kinase activity mediates proproliferative and thus protumorigenic effects in IECs (dashed red arrows). TRPV1 and PTP1B are predominantly expressed in the crypt compartment that contains TA cells (dark blue cells) with active EGFR signaling. Ligand-induced autophosphorylation of the EGFR results in PLC activation, which cleaves PIP_2, a tonic inhibitor of TRPV1, into diacylglycerol (DAG) and inositol triphosphate (IP_3; green arrows). This results in TRPV1 triggering and Ca^{2+} influx, which activates calpain and subsequently PTP1B. PTP1B then dephosphorylates EGFR (blue lines). This coupling between EGFR and TRPV1 exerts negative feedback on growth factor receptor signaling, inhibits crypt progenitor cell (dark blue cells) turnover, and hence reduces the risk of intestinal neoplasia development (red cells). +4 ISC, ISC at +4 position; CBCC, crypt-based columnar stem cell.

IECs (61), analogous to the increased rate of adenoma formation we observed in *Trpv1*$^{-/-}$ mice on the *Apc*$^{Min/+}$ background (Figure 7, A and B). We propose that both TRPV1 and Lrig1 are part of intrinsic feedback loops that restrain the proproliferative effects of EGFR in the intestinal epithelium, albeit with different operational modes. Whereas TRPV1 uses a PTP to downregulate EGFR activity (Figure 5, B–E), Lrig1 regulates EGFR degradation (60). Furthermore, Lrig1 expression is restricted to the intestinal stem cell population (32), whereas our data suggested a more diffuse expression pattern of TRPV1 in intestinal crypts (Figure 1, D and I). Thus, these 2 regulatory systems appear to act in a nonredundant fashion in the intestinal epithelium to suppress neoplasia development.

Our dissection of the intracellular components that negatively regulate EGFR activation downstream of TRPV1 outlined a requirement for the Ca^{2+}/calpain signaling axis and identified PTP1B as a key target of this pathway. PTP1B is a prototypical, nonreceptor PTP that directly interacts with the EGFR and dephosphorylates Tyr residues upon receptor activation (62, 63). This interaction occurs after endocytosis of the EGFR (39, 64), thus regulating its activity mostly downstream of receptor ligation. Our data suggest an additional pathway via TRPV1 and Ca^{2+}/calpain, which enhances PTP1B activity upon EGFR-TRPV1 triggering. Importantly, the effects of TRPV1 on EGFR^{Y1068} phosphorylation were recapitulated by expression of PTP1B C-terminal truncation mutants (Figure 5E), further supporting the calpain-PTP1B connection. A recent publication showed that metastasis-associated phosphatase of regenerating liver-3 (PRL-3) exerts protumorigenic effects in CRC by transcriptional downregulation of PTP1B (65). These data and ours are consistent with the proposed tumor-suppressive function of PTP1B in CRC. Indeed, PTP1B has been suggested to negatively regulate cell growth, prevent cellular transformation, strengthen cell-cell adhesions, promote apoptosis, and inhibit lymphomagenesis (37, 66, 67). However, PTP1B may also have protumorigenic effects by upregulating Ras-MAPK signaling, by directly activating the proto-oncogene c-Src (37, 68), and by promoting ErbB2-driven oncogenesis of mammary epithelial cells (68, 69). Thus, PTP1B appears to have paradoxical effects on ErbB1/EGFR and ErbB2-associated tumorigenesis. Since both pathways play a role in the pathogenesis of CRC (58), further studies on the role of PTP1B in intestinal tumorigenesis are warranted. Clinical use of PTP1B inhibitors was proposed for the prevention and/or treatment of insulin and leptin resistance (70), as well as breast cancer (71). However, this strategy must be approached with caution, as it could potentially promote the development of hematopoietic or intestinal neoplasia.

The role of TRPV1 as a tumor suppressor in the intestines is remarkable, as most TRP channels have been assigned oncogenic properties (including TRPC, TRPV, and TRPM family members; ref. 72), although the associated mechanistic aspects are largely unknown. A recent report by The Cancer Genome Atlas (TCGA) Network identified abundant somatic mutations in genes encoding calpains (*CAPN1–CAPN13*), PTP1B (*PTPN1*), TRPV1, and other TRP channels, demonstrating their importance in the pathogenesis of CRC (73). TRPV1 has been previously associated with regulation of EGFR signaling in the context of skin carcinogenesis (74). Our data differ from these findings in that we did not find any evidence for TRPV1-mediated EGFR degradation in IECs. We also identified an inverse correlation between EGFR^{Tyr1068} phosphorylation and TRPV1 expression. Thus, TRPV1 appears to mediate disparate effects, even in analogous epithelial tissues. This is also demonstrated by the recent finding that triggering of one of its close family members, TRPV3, actually promotes EGFR signaling in epithelial cells of the skin. This effect involves enhanced Ca^{2+}-dependent production and release of EGFR ligands (21). Although its expression is very low in IECs, TRPV3 also promoted EGFR signaling in our experimental system (Supplemental Figure 4C). However, the physiological mechanism of TRPV1 or TRPV3 channel gating in keratinocytes remains unclear. Finally, a protective role for TRPV1-mediated neurogenic inflammation was recently proposed in the etiology of colorectal tumorigenesis (46). Our data suggest that systemic (neonatal) ablation of TRPV1^{+} sensory neurons did not phenocopy the increased tumorigenesis observed in *Apc*$^{Min/+}$ *Trpv1*$^{-/-}$ mice (Figure 7, A–D, and Supplemental Figure 8, C and D). These data led us to propose a model whereby epithelial TRPV1 signaling regulates the EGFR pathway and its associated protumorigenic effects in the intestines (Figure 8).

In conclusion, our data suggest that TRPV1 senses and regulates cell proliferation in the intestinal epithelium. Mechanistically, we identified a novel pathway downstream of TRPV1 through Ca^{2+}/calpain and PTP1B that regulates cell growth signaling and affects IEC homeostasis and tumorigenesis. Our data also suggested that TRPV1 triggering by dietary administration of capsaicin suppressed intestinal tumorigenesis. Based on these results, we propose that the administration of TRPV1 agonists in combination with a COX-2 inhibitor may prevent the adenoma-to-carcinoma sequence in humans.

Methods

Reagents. Recombinant mEGF for in vitro and in vivo stimulations was purchased from PeproTech. DMSO, DTT, ATP, capsaicin (≥95% purity, from *Capsicum* sp.), and Na_3VO_4 were purchased from Sigma-Aldrich. Gefitinib, resiniferatoxin, and celecoxib were obtained from LC Labs. EDTA and G418 (Geneticin) were obtained from Invitrogen. Puromycin was obtained from InvivoGen. PIP_2 was purchased from Echelon (catalog no. P-4508). BCTC, W-7, and FK506 were obtained from Tocris. ALLM and the selective PTP1B inhibitor Compound 3 [3-(3,5-dibromo-4-hydroxy-benzoyl)-2-ethyl-benzofuran-6-sulfonic-acid-(4-(thiazol-2-ylsulfamyl)-phenyl)-amide; ref. 75] were obtained from Calbiochem. Alexa Fluor 488–conjugated wheat germ agglutinin, Alexa Fluor 546–conjugated phalloidin, and Alexa Fluor 488–conjugated secondary antibodies for immunostainings were obtained from Molecular Probes.

Antibodies. Anti–phospho-EGFR (Y992, Y1045, S1046/S1047, and Y1068), anti-EGFR, anti–phospho-ERK1/2 (T202/Y204), anti-ERK1/2, anti-PCNA, anti-MMP7, anti-PTP1B (for Western blotting), anti-synaptophysin, and anti-PLCγ1 antibodies were from Cell Signaling Technologies; anti–β-actin antibody was from Sigma-Aldrich; anti-Ki67 was from Abcam; and anti-occludin was from Neomarkers. Anti-PTP1B antibody for immunohistochemistry was obtained from Epitomics. Anti-TRPV1 antibody (P-19) and corresponding blocking peptide for Western blotting and flow cytometry were obtained from Santa Cruz Biotechnology Inc. Anti-TRPV1 antibody for immunofluorescent stainings was obtained from Alomone Labs (catalog no. ACC-030). Anti–phospho-Hrs (Y334) antibody was provided by S. Urbé (University of Liverpool, Liverpool, United Kingdom; ref. 40).

Cell culture, in vitro assays, and transfections. HCT116, HEK293, IEC-6, and CMT-93 cells were cultured in high-glucose DMEM (Mediatech); HCA-7 cells were cultured in low-glucose DMEM. Culture medium was supplemented with 4 mM glutamine, 10% fetal calf serum, 50 U/ml penicillin, and 50 μg/ml streptomycin. The rTRPV1 (pcDNA3) and mTRPV3 (pcDNA5) plasmids, CHO^{K1} cell line, and stable CHO^{TRPV1} transgenic cell line were provided by A. Patapoutian (Scripps Research Institute, La Jolla, California, USA). CHO^{TRPV1} cells were maintained in G418-containing selection medium. The WT-EGFR (pLWERNL) plasmid was provided by F. Furnari (UCSD, La Jolla, California, USA), the mTRPV4-FLAG (pcDNA3) plasmid was provided by G. Walz (University Hospital Freiburg, Freiburg, Germany), and the rbTRPV5 (pEGFP-N3) plasmid was provided by C.-L. Huang (UT Southwestern, Dallas, Texas, USA). Plasmids containing HA-tagged human full-length PTP1B (pJ3H-PTP435) and C-terminal truncation mutants pJ3H-PTP370 (aa 1–370) and pJ3H-PTP377 (aa 1–377) were donated by J. Chernoff (Fox Chase Cancer Center, Philadelphia, Pennsylvania, USA). CHO and HCT116 cells were transfected with WT-EGFR and/or TRPV1, TRPV3, TRPV4, TRPV5, or PTP1B plasmids (1–3 μg DNA per 10^6 cells) with Nucleofector (Amaxa), as previously described (76). Cells were serum-starved 2–4 hours before EGF stimulation (1–10 ng/ml, as indicated). In some conditions, cells were pretreated for 1 hour with W-7 (10 μM), FK506 (1–10 μM), Na_3VO_4 (10 μM), Compound 3 (10 μM), ALLM (10 μM), or DMSO. MTT assay (Sigma-Aldrich) was performed according to the manufacturer's instructions. Knockdown in HCT116 and HEK293 cells was performed with Nucleofector. *TRPV1* shRNA consisted of a pool of 3 independent, target-specific shRNAs: sc-36826-SHA (GATCCGAAGACCTGTCTGCTGAAATTCAAGAGATTTCAGCAGACAGGTCTTCTTTTT) and corresponding siRNA sequences (sc-36826A) (sense, GAAGACCUGUCUGCUGAAATT; antisense, UUUCAGCAGACAGGUCUUCTT), sc-36826-SHB (GATCCCGAGCATGTACAATGAGATTTCAAGAGAATCTCATTGTACATGCTCGTTTTT) and corresponding siRNA sequences (sc-36826B) (sense, CGAGCAUGUACAAUGAGAUTT; antisense, AUCUCAUUGUACAUGCUCGTT), and sc-36826-SHC (GATCCCGCATCTTCTACTTCAACTTTCAAGAGAAGTTGAAGTAGAAGATGCGTTTTT) and corresponding siRNA sequences (sc-36826C) (sense, CGCAUCUUCUACUUCAACUTT; antisense, AGUUGAAGUAGAAGAUGCGTT). *TRPV1* siRNA consisted of a pool of 3 different siRNA duplexes: sc-36826A, sc-36826B, and sc-36826C. *PTP1B* siRNA consisted of a pool of 3 different siRNA duplexes: sc-36328A (sense, CUUCCGUUGAUAUCAAGAATT; antisense, UUCUUGAUAUCAACGGAAGTT), sc-36328B (sense, GCAUGACCUGAUCAUUACATT; antisense, UGUAAUGAUCAGGUCAUGCTT), and sc-36328C (sense, CUCCGCCAUUCCAAGUCAATT; antisense, UUGACUUGGAAUGGCGGAGTT). *PLCG1* siRNA consisted of a pool of 4 different siRNA duplexes: sc-29452A (sense, CAAACCCUAUGCCAACUUUTT; antisense, AAAGUUGGCAUAGGGUUUGTT), sc-29452B (sense, GCAAGAAGUUCCUUCAGUATT; antisense, UACUGAAGGAACUUCUUGCTT), sc-29452C (sense, ACAGAGCAGUGCCUUUGAATT; antisense, UUCAAAGGCACUGCUCUGUTT), and sc-29452D (sense, CAAACCUACUGCCCACAUUTT; antisense, AAUGUGGGCAGUAGGUUUGTT). shRNA and siRNA sequences were purchased from Santa Cruz. Nontargeting control shRNA lentiviral particles (copGFP Control Lentiviral Particles; Santa Cruz) or control siRNA (nontargeting siRNA #2; Dharmacon) were used as controls. Knockdown with shRNA was followed by puromycin selection and functional validation.

Mice and in vivo intervention studies. To conditionally overexpress TRPV1 in IECs in mice, the *ROSA-stop^{flox}-TRPV1-IRES-ECFP* strain (31) was crossed to Villin-Cre mice. *$Apc^{Min/+}$ $Trpv1^{-/-}$* mice were generated by crossing *$Apc^{Min/+}$* mice with *$Trpv1^{-/-}$* mice (26). Follow-up and health monitoring of *$Apc^{Min/+}$* mice was performed as previously published (7). All mouse strains were on the C57BL/6J background and obtained from The Jackson Laboratory. Gefitinib, reconstituted in DMSO, was delivered by gavage in 0.05% (hydroxypropyl)methylcellulose and 0.02% Tween 80 vehicle at 50 mg/kg according to the indicated dosing schedules. For dietary studies, C57BL/6J mice were fed standard laboratory chow or chow mixed with 0.01% (w/w) capsaicin ad libitum (77) for the indicated time periods. *$Apc^{Min/+}$* and *$Apc^{Min/+}$ $Trpv1^{-/-}$* mice received normal chow (control) or chow plus 0.01% (w/w) capsaicin ad libitum starting at 8 weeks of age and were followed for survival studies or until they reached 20 weeks of age. Other cohorts of *$Apc^{Min/+}$* mice received low-dose celecoxib (300 ppm) mixed with chow (78), with or without 0.01% (w/w) capsaicin ad libitum. Chow was prepared

freshly every week. For neonatal TRPV1$^+$ sensory neuron ablation, *Apc*$^{Min/+}$ mice were treated with resiniferatoxin (50 μg/kg s.c.) on days 1, 2, and 7 after birth. Validation of systemic TRPV1$^+$ neuronal ablation was performed with the eye wipe test by ocular challenge with 0.01% (w/v) capsaicin in saline (47).

Intestinal organoid culture and immunofluorescent staining. Mouse intestinal organoids were generated from small intestines, following published protocols (23). Organoids were maintained in ENR (EGF, Noggin, RspoI) medium, which consisted of Advanced DMEM/F12 Reduced Serum Medium (Invitrogen) supplemented with 2 mM GlutaMAX, 10 mM HEPES, 100 U/ml penicillin and 100 μg/ml streptomycin, and B27 and N2 supplements (Invitrogen) with 50 ng/ml mEGF (Invitrogen), 100 ng/ml mNoggin (PeproTech), and 10% (v/v) RspoI conditioned medium. RspoI conditioned medium was generated using the 293T-HA-RspoI-Fc cell line (provided by C. Kuo, Stanford University, Stanford, California, USA). Matrigel (GFR) was obtained from BD Biosciences. WT and *Trpv1*$^{-/-}$ organoids at similar developmental stages in parallel cultures were compared in the analyses. For EGF starvation experiments, EGF was removed from the culture medium 2 days after passing, for a period of 48 hours before analysis. For immunofluorescent stainings, organoids were grown in Matrigel and stained in 8-well chamber slides (Nunc). Immunofluorescent stainings were performed using anti-TRPV1 (Alomone Labs), anti-MMP7 (Cell Signaling), anti-Ki67 (Abcam), or anti-PTP1B (Epitomics) primary Abs. Briefly, fixed organoids in Matrigel were stained with primary Abs (1:100 dilution) and detected with Alexa Fluor 488–conjugated anti-Rb secondary antibody (1:500 dilution). After counterstaining with Alexa Fluor 546–conjugated phalloidin and DAPI, organoids were analyzed by confocal fluorescence microscopy. Staining with Alexa Fluor 488–conjugated wheat germ agglutinin and Alexa Fluor 546–conjugated phalloidin were performed according to the manufacturer's instructions. For Q-PCR analysis, organoids were extracted from Matrigel using BD Cell Recovery Solution following the manufacturer's instructions.

Ca^{2+} imaging. Ca^{2+} imaging was performed as previously described (28, 29). Briefly, for imaging with cell lines (CHO, HEK293, or HCT116), cells were grown on coverslips and loaded with 5 μM Fura-2 AM (Invitrogen) dissolved in 0.01% Pluronic F-127 (Invitrogen) plus 0.1% DMSO in physiological salt solution (140 mM Na^+, 5 mM K^+, 2 mM Ca^{2+}, 147 mM Cl^-, 10 mM HEPES, and 10 mM glucose, pH 7.4) at room temperature (20°C) for 1 hour. Cells were then washed for 0.5 hours, mounted in a perfusion chamber on a Nikon microscope stage, and perfused with PSS. After obtaining baseline measurements at room temperature, cells were then stimulated with capsaicin, heated PSS (up to 40°C), or EGF (100 ng/ml). ATP (10 μM) was used as a positive control for $[Ca^{2+}]_{cyt}$ measurements. In some conditions, cells were pretreated with either the TRPV1 antagonist BCTC (1–10 μM) or PIP_2 (30 μM) for 30 minutes. For Ca^{2+} imaging with intestinal organoids, organoids generated from WT and *Trpv1*$^{-/-}$ mice were passed and seeded 1 day before imaging. On the day of analysis, organoids were recovered from Matrigel, stained with 5 μM Fura-2 AM (1 hour), washed, attached on BD Cell-Tek–coated coverslips, and stimulated with capsaicin (30 μM). Data are shown as mean ± SEM from individual $[Ca^{2+}]_{cyt}$ measurements based on recordings of $F_{340/380\ nm}$ ratios.

IEC isolation and ex vivo stimulation. Colons or small intestines were opened longitudinally, and feces were removed without scraping. Intestines were then washed in PBS (1 mM DTT) on ice. Intestines were minced into 3- to 5-mm pieces and incubated in HBSS (5 mM EDTA, 10 mM HEPES, and 0.5 mM DTT) in conical 50-ml tubes for 1 hour at 37°C. Intestinal pieces were then vigorously shaken (15 seconds) to detach crypts. The supernatants containing IECs were separated from larger pieces of nonepithelial tissue and spun. Pellets were washed in PBS, resuspended in lysis buffer, and stored at –80°C until protein or RNA analysis. IEC fractionation was performed following published protocols (79). Briefly, small intestines from WT mice were fractionated in 2 villus fractions (from distal to proximal along the crypt-villus axis) and 1 crypt fraction. For ex vivo stimulation of IECs, colons were cut open longitudinally and washed in PBS on ice. They were cut in halves and stimulated with or without EGF (50 ng/ml) for 15 minutes (37°C). Immediately after EGF stimulation, IEC isolation was performed (all steps on ice), and crypts were lysed in total cell lysis buffer for Western blot analysis.

Flow cytometry. TRPV1 antibodies were preincubated with 10-fold excess of blocking peptide or PBS. Cells were then stained with anti-TRPV1 (diluted 1:100) or goat IgG for 1 hour at 4°C. Primary goat anti-TRPV1 Abs were detected with rabbit anti-goat secondary Abs (Alexa Fluor 488 conjugate). Cells were run on a BD FACSCalibur flow cytometer or Accuri C6 (BD Biosciences).

Immunohistochemistry. Immunohistochemistry was performed as described previously (7), with minor modifications. Briefly, 4- to 6-μm paraffin sections from murine ileums or colons were incubated with anti-Ki67, anti-MMP7, anti–phospho-EGFR, or anti-PTP1B antibodies overnight. Abs were detected with biotinylated secondary Abs, HRP-streptavidin conjugates (Jackson), and visualized with DAB (Vector Laboratories). Counterstaining was performed with Hematoxylin 560 (Surgipath). The Alcian Blue–P.A.S. Stain kit was obtained from American MasterTech, and stainings were performed according to the manufacturer's instructions. The NanoZoomer 2.0-HT (Hamamatsu) slide scanner and NanoZoomer Digital Pathology software was used for histological analyses. Image analysis was performed with ImageJ (version 1.47) with the Colour Deconvolution or ImmunoRatio plugin (version 1.0c).

Q-PCR and gel electrophoresis. RNA isolation was performed with the RNeasy Mini Kit or Micro Kit (Qiagen), and cDNA synthesis was performed with the qScript cDNA superMix kit (Quanta Biosciences) or the RT~ First Strand Kit (Qiagen). Q-PCR was performed on the AB7300 Real-Time PCR System (Applied Biosytems) using PerfeCta SYBR Green FastMix (Quanta Biosciences) or a Roche Lightcycler 480 using SYBR Green qPCR Master Mix (SaBiosciences/Qiagen). The custom-designed oligonucleotide sequences (IDT Technologies) used for Q-PCR are summarized in Supplemental Tables 1 and 2. *Ptpn1* (NM_011201), *Ptpn2* (NM_001127177, NM_008977), *Ptpn6* (NM_001077705, NM_013545), *Ptprf* (NM_011213), and *Ptprs* (NM_001252453, NM_001252455, NM_001252456, NM_011218) primer sets were obtained from SABiosciences/Qiagen. PCR products were run on 2% agarose gels and visualized with SYBR Safe DNA (Invitrogen).

Statistics. Data are presented as mean ± SD or mean ± SEM, as indicated. Unpaired, 2-tailed Student's *t* test was used for statistical analyses to compare 2 data sets with normal distribution, with the exception of Figure 4, C and F (1-tailed Student's *t* test); Mann-Whitney *U* test was used for nonparametric data; ANOVA was used to compare multiple data sets; and log-rank analysis was applied for survival curves (GraphPad Prism 5.0). A *P* value less than 0.05 was considered significant.

Study approval. All experimental procedures involving mice were reviewed and approved by the UCSD Institutional Animal Care and Use Committee (IACUC; animal protocol no. S02240).

Acknowledgments

We thank P. Charos and M. Scholl (UCSD Animal Genetics Core Facility) for animal breeding, L. Deng and S. Shenouda for tissue processing, N. Varki (Department of Pathology, UCSD) for histological evaluations, S. van den Brink (Hubrecht Institute, KNAW, Utrecht, The Netherlands) for assistance with organoid cultures, and J. Santini (UCSD Neuroscience Microscopy Shared Facility, funded by NINDS, NIH, grant P30 NS047101) for assistance with confocal imaging. This study was supported by grants from the Crohn's and Colitis Foundation of America to P.R. de Jong (The contribution of neurogenic inflammation to Inflammatory Bowel Disease; RFA2927), S. Bertin (RFA3574), and E. Raz (Senior Research Award); by the Prins Bernhard Cultural Foundation, the Scholten-Cordes Foundation, the Dr. Hendrik Muller Vaderlandsch Foundation, and a VSBfund Nuffic Scholarship to P.R. de Jong; by the Japan Society for the Promotion of Science to N. Takahashi; by the European Molecular Biology Organization to S. Bertin; by a Fellowship of the Juvenile Diabetes Research Foundation to S.M. Stanford; by the Strategic Young Researcher Overseas Visits Program for Accelerating Brain Circulation to K. Taniguchi; by the Broad Medical Foundation to E. Raz; and by the NIH (AI095623 and DK35108).

Address correspondence to: Eyal Raz, University of California, San Diego, 9500 Gilman Dr., La Jolla, California 92093-0663, USA. Phone: 858.534.5444; E-mail: eraz@ucsd.edu.

1. van der Flier LG, Clevers H. Stem cells, self-renewal, and differentiation in the intestinal epithelium. *Annu Rev Physiol*. 2009;71:241–260.
2. Schwitalla S, et al. Intestinal tumorigenesis initiated by dedifferentiation and acquisition of stem-cell-like properties. *Cell*. 2013;152(1–2):25–38.
3. Sato T, et al. Paneth cells constitute the niche for Lgr5 stem cells in intestinal crypts. *Nature*. 2011;469(7330):415–418.
4. Radtke F, Clevers H. Self-renewal and cancer of the gut: two sides of a coin. *Science*. 2005;307(5717):1904–1909.
5. Markowitz SD, Bertagnolli MM. Molecular origins of cancer: Molecular basis of colorectal cancer. *N Engl J Med*. 2009;361(25):2449–2460.
6. Abreu MT. Toll-like receptor signalling in the intestinal epithelium: how bacterial recognition shapes intestinal function. *Nat Rev Immunol*. 2010;10(2):131–144.
7. Lee SH, et al. ERK activation drives intestinal tumorigenesis in Apc(min/+) mice. *Nat Med*. 2010;16(6):665–670.
8. Medema JP, Vermeulen L. Microenvironmental regulation of stem cells in intestinal homeostasis and cancer. *Nature*. 2011;474(7351):318–326.
9. Madison BB, Braunstein K, Kuizon E, Portman K, Qiao XT, Gumucio DL. Epithelial hedgehog signals pattern the intestinal crypt-villus axis. *Development*. 2005;132(2):279–289.
10. Batts LE, Polk DB, Dubois RN, Kulessa H. Bmp signaling is required for intestinal growth and morphogenesis. *Dev Dyn*. 2006;235(6):1563–1570.
11. Zacharias WJ, et al. Hedgehog signaling controls homeostasis of adult intestinal smooth muscle. *Dev Biol*. 2011;355(1):152–162.
12. He XC, et al. BMP signaling inhibits intestinal stem cell self-renewal through suppression of Wnt-β-catenin signaling. *Nat Genet*. 2004;36(10):1117–1121.
13. Haramis AP, et al. De novo crypt formation and juvenile polyposis on BMP inhibition in mouse intestine. *Science*. 2004;303(5664):1684–1686.
14. Eisenhoffer GT, et al. Crowding induces live cell extrusion to maintain homeostatic cell numbers in epithelia. *Nature*. 2012;484(7395):546–549.
15. Wu LJ, Sweet TB, Clapham DE. International Union of Basic and Clinical Pharmacology. LXXVI. Current progress in the mammalian TRP ion channel family. *Pharmacol Rev*. 2010;62(3):381–404.
16. Minke B. The history of the Drosophila TRP channel: the birth of a new channel superfamily. *J Neurogenet*. 2010;24(4):216–233.
17. Holzer P. Transient receptor potential (TRP) channels as drug targets for diseases of the digestive system. *Pharmacol Ther*. 2011;131(1):142–170.
18. Birder LA, et al. Vanilloid receptor expression suggests a sensory role for urinary bladder epithelial cells. *Proc Natl Acad Sci U S A*. 2001;98(23):13396–13401.
19. Peier AM, et al. A heat-sensitive TRP channel expressed in keratinocytes. *Science*. 2002;296(5575):2046–2049.
20. Shapovalov G, Lehen'kyi V, Skryma R, Prevarskaya N. TRP channels in cell survival and cell death in normal and transformed cells. *Cell Calcium*. 2011;50(3):295–302.
21. Cheng X, et al. TRP channel regulates EGFR signaling in hair morphogenesis and skin barrier formation. *Cell*. 2010;141(2):331–343.
22. Tajeddine N, Gailly P. TRPC1 protein channel is major regulator of epidermal growth factor receptor signaling. *J Biol Chem*. 2012;287(20):16146–16157.
23. Sato T, et al. Single Lgr5 stem cells build crypt-villus structures in vitro without a mesenchymal niche. *Nature*. 2009;459(7244):262–265.
24. D'Aldebert E, et al. Transient receptor potential vanilloid 4 activated inflammatory signals by intestinal epithelial cells and colitis in mice. *Gastroenterology*. 2011;140(1):275–285.
25. van Abel M, Hoenderop JG, van der Kemp AW, van Leeuwen JP, Bindels RJ. Regulation of the epithelial Ca^{2+} channels in small intestine as studied by quantitative mRNA detection. *Am J Physiol Gastrointest Liver Physiol*. 2003;285(1):G78–G85.
26. Caterina MJ, et al. Impaired nociception and pain sensation in mice lacking the capsaicin receptor. *Science*. 2000;288(5464):306–313.
27. Clapham DE. TRP channels as cellular sensors. *Nature*. 2003;426(6966):517–524.
28. Dong X, et al. P2Y receptors mediate Ca2+ signaling in duodenocytes and contribute to duodenal mucosal bicarbonate secretion. *Am J Physiol Gastrointest Liver Physiol*. 2009;296(2):G424–G432.
29. Lee YS, et al. The fractalkine/CX3CR1 system regulates β cell function and insulin secretion. *Cell*. 2013;153(2):413–425.
30. Jimeno A, et al. C-fos assessment as a marker of anti-epidermal growth factor receptor effect. *Cancer Res*. 2006;66(4):2385–2390.
31. Arenkiel BR, Klein ME, Davison IG, Katz LC, Ehlers MD. Genetic control of neuronal activity in mice conditionally expressing TRPV1. *Nat Methods*. 2008;5(4):299–302.
32. Wong VW, et al. Lrig1 controls intestinal stem-cell homeostasis by negative regulation of ErbB signalling. *Nat Cell Biol*. 2012;14(4):401–408.
33. Sanchez-Gonzalez P, Jellali K, Villalobo A. Calmodulin-mediated regulation of the epidermal growth factor receptor. *FEBS J*. 2010;277(2):327–342.
34. Sullivan KM, Rubin GM. The Ca(2+)-calmodulin-activated protein phosphatase calcineurin negatively regulates EGF receptor signaling in Drosophila development. *Genetics*. 2002;161(1):183–193.
35. Avraham R, Yarden Y. Feedback regulation of EGFR signalling: decision making by early and delayed loops. *Nat Rev Mol Cell Biol*. 2011;12(2):104–117.
36. Ostman A, Bohmer FD. Regulation of receptor tyrosine kinase signaling by protein tyrosine phosphatases. *Trends Cell Biol*. 2001;11(6):258–266.
37. Yip SC, Saha S, Chernoff J. PTP1B: a double agent in metabolism and oncogenesis. *Trends Biochem Sci*. 2010;35(8):442–449.
38. Cortesio CL, et al. Calpain 2 and PTP1B function in a novel pathway with Src to regulate invadopodia dynamics and breast cancer cell invasion. *J Cell Biol*. 2008;180(5):957–971.
39. Eden ER, White IJ, Tsapara A, Futter CE. Membrane contacts between endosomes and ER provide sites for PTP1B-epidermal growth factor receptor interaction. *Nat Cell Biol*. 2010;12(3):267–272.
40. Urbe S, et al. The UIM domain of Hrs couples receptor sorting to vesicle formation. *J Cell Sci*. 2003;116(pt 20):4169–4179.
41. McCole DF, Truong A, Bunz M, Barrett KE. Consequences of direct versus indirect activation of epidermal growth factor receptor in intestinal epithelial cells are dictated by protein-tyrosine phosphatase 1B. *J Biol Chem*. 2007;282(18):13303–13315.
42. Prescott ED, Julius D. A modular PIP2 binding site as a determinant of capsaicin receptor sensitivity. *Science*. 2003;300(5623):1284–1288.
43. Cao E, Cordero-Morales JF, Liu B, Qin F, Julius D.

TRPV1 channels are intrinsically heat sensitive and negatively regulated by phosphoinositide lipids. *Neuron*. 2013;77(4):667–679.
44. Haugh JM, Schooler K, Wells A, Wiley HS, Lauffenburger DA. Effect of epidermal growth factor receptor internalization on regulation of the phospholipase C-γ1 signaling pathway. *J Biol Chem*. 1999;274(13):8958–8965.
45. Roberts RB, et al. Importance of epidermal growth factor receptor signaling in establishment of adenomas and maintenance of carcinomas during intestinal tumorigenesis. *Proc Natl Acad Sci U S A*. 2002;99(3):1521–1526.
46. Vinuesa AG, et al. Vanilloid receptor-1 regulates neurogenic inflammation in colon and protects mice from colon cancer. *Cancer Res*. 2012;72(7):1705–1716.
47. Pecze L, et al. Resiniferatoxin mediated ablation of TRPV1+ neurons removes TRPA1 as well. *Can J Neurol Sci*. 2009;36(2):234–241.
48. Bertagnolli MM, et al. Celecoxib for the prevention of sporadic colorectal adenomas. *N Engl J Med*. 2006;355(9):873–884.
49. Pai R, Soreghan B, Szabo IL, Pavelka M, Baatar D, Tarnawski AS. Prostaglandin E2 transactivates EGF receptor: a novel mechanism for promoting colon cancer growth and gastrointestinal hypertrophy. *Nat Med*. 2002;8(3):289–293.
50. Caterina MJ, Schumacher MA, Tominaga M, Rosen TA, Levine JD, Julius D. The capsaicin receptor: a heat-activated ion channel in the pain pathway. *Nature*. 1997;389(6653):816–824.
51. Hwang SW, et al. Direct activation of capsaicin receptors by products of lipoxygenases: endogenous capsaicin-like substances. *Proc Natl Acad Sci U S A*. 2000;97(11):6155–6160.
52. Chuang HH, Lin S. Oxidative challenges sensitize the capsaicin receptor by covalent cysteine modification. *Proc Natl Acad Sci U S A*. 2009;106(47):20097–20102.
53. Chuang HH, et al. Bradykinin and nerve growth factor release the capsaicin receptor from PtdIns(4,5)P2-mediated inhibition. *Nature*. 2001;411(6840):957–962.
54. Waning J, et al. A novel function of capsaicin-sensitive TRPV1 channels: involvement in cell migration. *Cell Calcium*. 2007;42(1):17–25.
55. Rohacs T, Nilius B. Regulation of transient receptor potential (TRP) channels by phosphoinositides. *Pflugers Arch*. 2007;455(1):157–168.
56. Dimke H, Hoenderop JG, Bindels RJ. Molecular basis of epithelial Ca2+ and Mg2+ transport: insights from the TRP channel family. *J Physiol*. 2011;589(pt 7):1535–1542.
57. Groenestege WM, et al. Impaired basolateral sorting of pro-EGF causes isolated recessive renal hypomagnesemia. *J Clin Invest*. 2007; 117(8):2260–2267.
58. Fiske WH, Threadgill D, Coffey RJ. ERBBs in the gastrointestinal tract: recent progress and new perspectives. *Exp Cell Res*. 2009;315(4):583–601.
59. Segatto O, Anastasi S, Alema S. Regulation of epidermal growth factor receptor signalling by inducible feedback inhibitors. *J Cell Sci*. 2011;124(pt 11):1785–1793.
60. Laederich MB, et al. The leucine-rich repeat protein LRIG1 is a negative regulator of ErbB family receptor tyrosine kinases. *J Biol Chem*. 2004;279(45):47050–47056.
61. Powell AE, et al. The pan-ErbB negative regulator Lrig1 is an intestinal stem cell marker that functions as a tumor suppressor. *Cell*. 2012;149(1):146–158.
62. Liu F, Chernoff J. Protein tyrosine phosphatase 1B interacts with and is tyrosine phosphorylated by the epidermal growth factor receptor. *Biochem J*. 1997;327(pt 1):139–145.
63. Haj FG, Markova B, Klaman LD, Bohmer FD, Neel BG. Regulation of receptor tyrosine kinase signaling by protein tyrosine phosphatase-1B. *J Biol Chem*. 2003;278(2):739–744.
64. Haj FG, Verveer PJ, Squire A, Neel BG, Bastiaens PI. Imaging sites of receptor dephosphorylation by PTP1B on the surface of the endoplasmic reticulum. *Science*. 2002;295(5560):1708–1711.
65. Al-Aidaroos AQ, et al. Metastasis-associated PRL-3 induces EGFR activation and addiction in cancer cells. *J Clin Invest*. 2013;123(8):3459–3471.
66. Dubé N, et al. Genetic ablation of protein tyrosine phosphatase 1B accelerates lymphomagenesis of p53-null mice through the regulation of B-cell development. *Cancer Res*. 2005;65(21):10088–10095.
67. Lessard L, Stuible M, Tremblay ML. The two faces of PTP1B in cancer. *Biochim Biophys Acta*. 2010;1804(3):613–619.
68. Bentires-Alj M, Neel BG. Protein-tyrosine phosphatase 1B is required for HER2/Neu-induced breast cancer. *Cancer Res*. 2007;67(6):2420–2424.
69. Julien SG, et al. Protein tyrosine phosphatase 1B deficiency or inhibition delays ErbB2-induced mammary tumorigenesis and protects from lung metastasis. *Nat Genet*. 2007;39(3):338–346.
70. St-Pierre J, Tremblay ML. Modulation of leptin resistance by protein tyrosine phosphatases. *Cell Metab*. 2012;15(3):292–297.
71. Tonks NK, Muthuswamy SK. A brake becomes an accelerator: PTP1B — a new therapeutic target for breast cancer. *Cancer Cell*. 2007;11(3):214–216.
72. Lehen'kyi V, Prevarskaya N. Oncogenic TRP channels. *Adv Exp Med Biol*. 2011;704:929–945.
73. Cancer Genome Atlas Network. Comprehensive molecular characterization of human colon rectal cancer. *Nature*. 2012;487(7407):330–337.
74. Bode AM, et al. Transient receptor potential type vanilloid 1 suppresses skin carcinogenesis. *Cancer Res*. 2009;69(3):905–913.
75. Wiesmann C, et al. Allosteric inhibition of protein tyrosine phosphatase 1B. *Nat Struct Mol Biol*. 2004;11(8):730–737.
76. Lee J, et al. Signal transducer and activator of transcription 3 (STAT3) protein suppresses adenoma-to-carcinoma transition in Apcmin/+ mice via regulation of Snail-1 (SNAI) protein stability. *J Biol Chem*. 2012;287(22):18182–18189.
77. Yang D, et al. Activation of TRPV1 by dietary capsaicin improves endothelium-dependent vasorelaxation prevents hypertension. *Cell Metab*. 2010;12(2):130–141.
78. Swamy MV, Patlolla JM, Steele VE, Kopelovich L, Reddy BS, Rao CV. Chemoprevention of familial adenomatous polyposis by low doses of atorvastatin and celecoxib given individually and in combination to APCMin mice. *Cancer Res*. 2006;66(14):7370–7377.
79. Barker N, et al. Identification of stem cells in small intestine and colon by marker gene Lgr5. *Nature*. 2007;449(7165):1003–1007.